Journal of Innovative Optical Health Sciences
Vol. 7, No. 5 (2014) 1330009 (22 pages)
© The Authors
DOI: 10.1142/S1793545813300097

World Scientific
www.worldscientific.com

J. Innov. Opt. Health Sci. 2014.07. Downloaded from www.worldscientific.com
by 103.240.126.9 on 10/21/18. Re-use and distribution is strictly not permitted, except for Open Access articles.

# Multimodal label-free microscopy

Nicolas Pavillon*,‡, Katsumasa Fujita†
and Nicholas Isaac Smith*,§
*Biophotonics Laboratory
Immunology Frontier Research Center (IFReC)
†Department of Applied Physics
Osaka University, Suita, Osaka 565-0871, Japan
‡nicolas.pavillon@a3.epfl.ch
§nsmith@ap.eng.osaka-u.ac.jp

Received 14 July 2013
Accepted 21 September 2013
Published 12 December 2013

This paper reviews the different multimodal applications based on a large extent of label-free imaging modalities, ranging from linear to nonlinear optics, while also including spectroscopic measurements. We put specific emphasis on multimodal measurements going across the usual boundaries between imaging modalities, whereas most multimodal platforms combine techniques based on similar light interactions or similar hardware implementations. In this review, we limit the scope to focus on applications for biology such as live cells or tissues, since by their nature of being alive or fragile, we are often not free to take liberties with the image acquisition times and are forced to gather the maximum amount of information possible at one time. For such samples, imaging by a given label-free method usually presents a challenge in obtaining sufficient optical signal or is limited in terms of the types of observable targets. Multimodal imaging is then particularly attractive for these samples in order to maximize the amount of measured information. While multimodal imaging is always useful in the sense of acquiring additional information from additional modes, at times it is possible to attain information that could not be discovered using any single mode alone, which is the essence of the progress that is possible using a multimodal approach.

*Keywords*: Optical microscopy; nonlinear optics; microspectroscopy.

## 1. Introduction

Label-free imaging implies the measurement of biological samples such as live cells or tissues without employing exogenous contrast agents, as opposed to imaging techniques such as fluorescence or histological staining. This requires that the retrieved signal originates directly from the interaction between the excitation light and the sample, an interaction which

‡,§Corresponding authors.

This is an Open Access article published by World Scientific Publishing Company. It is distributed under the terms of the Creative Commons Attribution 3.0 (CC-BY) License. Further distribution of this work is permitted, provided the original work is properly cited.

J. Innov. Opt. Health Sci. 2014.07. Downloaded from www.worldscientific.com
by 103.240.126.9 on 10/21/18. Re-use and distribution is strictly not permitted, except for Open Access articles.

can stem from a variety of physical processes, such as forward- or backscattering, molecular vibrational response, nonlinear effects, etc. It is not directly possible in label-free imaging to achieve the same level of specificity common in fluorescence imaging where chemically active probes can be employed to target specific molecules. Instead, the endogenous interaction of light with the observed sample can provide invaluable information about its structure and molecular composition, based on the analysis of the imaging contrast, while enabling the observation of any specimen without further modification, or interaction with additional chemical agents.

The use of multimodal imaging can significantly increase the amount of information extracted from a sample, by providing various imaging possibilities, and potentially multiplex measurements of spatial and chemical distributions in the specimen. Measuring several different channels in the case of label-free imaging can however be a challenging task, for example due to the absence of known emission spectra on which to base a choice of filters for spectral separation of modes, or because of the small cross-section of the observed interaction, which then provides only a weak signal.

Furthermore, while certain label-free methods can readily be observed simultaneously thanks to the use of similar optical configurations, imaging modalities originating from rather different physical light-sample interactions can be more challenging to combine. However, these implementations can potentially be the most promising candidates in terms of the quantity and variety of information which can be extracted from the sample using a multimodal implementation, thanks to their different physical interactions leading to differing sources of image contrast.

This paper reviews existing label-free imaging modalities, organized in terms of the type of interaction with the sample. We focus in particular on the multimodal applications which can provide additional and hopefully simultaneous information from the sample. Label-free imaging is considered here in a very broad sense, so that a large variety of imaging techniques are discussed. The description of each modality then cannot be exhaustive, as each label-free mode has an already extensive literature, and is usually described in reviews of its own. We therefore focus on the results provided by each technique, with particular attention to the view of multimodal imaging, and do not discuss in any detail the underlying physical processes and technical requirements of each of them. Similarly, some recent promising methods that have not yet been fully validated for biological imaging and currently employ very specific interactions or are only used for very specific applications are not necessarily treated in this paper.

The considered techniques belong in a broad sense to optical microscopy, i.e., have the ability to provide an image of the specimen (typically live cells, tissues or tissue sections), with microscopic resolution, and with wavelengths typically ranging in the visible and near infrared range. Furthermore, multimodal applications are considered in the sense that each mode can retrieve complementary information about the sample in a repetitive way and within a relatively short amount of time, ideally simultaneously with the other mode, so that the measurement is considered to be rapid and repeatable.

In Sec. 2, the different imaging modalities are briefly described, by classifying them through their interaction type with the sample, and by focusing on the type of measurement and contrast provided by each mode. Then, in Sec. 3, the different existing label-free multimodal applications are reviewed, first within a category, and then between categories. Then, although we focus on label-free multimodal techniques, label-based techniques such as fluorescence have a tremendous importance in present microscopy. The combination of label-free techniques with label-based ones are therefore briefly explored in Sec. 4, with an emphasis on recent developments in this area.

## 2. Label-Free Imaging Modalities

In this section, we present briefly the different label-free imaging methods developed for microscopy. As mentioned above, the focus of this review is the multimodal combinations; each individual method already has an extensive literature and is therefore only briefly described, with references to existing literature and reviews. The various imaging modalities are classified under larger categories to simplify the description, where these categories were chosen to order the different methods through the type of information and contrast they provide, along with their general physical interaction with the sample.

J. Innov. Opt. Health Sci. 2014.07. Downloaded from www.worldscientific.com
by 103.240.126.9 on 10/21/18. Re-use and distribution is strictly not permitted, except for Open Access articles.

### 2.1. *White light methods*

The first microscopy methods historically available to observe live cells and tissue sections are based on white light imaging, essentially due to the light sources available at that time. However, as biological samples usually exhibit low contrast through absorption, several methods were developed in order to retrieve a higher contrast when imaging these thin preparations. Most of these methods are relying on additional components to modify the observed part of light interacting with the sample. Among these approaches, the most known ones are phase-contrast microscopy[1] and differential interference contrast (DIC),[2] which enhance the contrast by observing phase components through optical manipulation. Another approach consists in observing only highly diffractive elements such as small organelles in the sample with dark-field microscopy, where the light directly transmitted through the sample is obstructed, leading to background-free images of the smaller and highly scattering features in the sample.

A last widely used method is based on polarization-resolved measurements, which makes it possible to highlight with high contrast birefringent materials such as crystals, by indirectly measuring the change of polarization induced by the sample.[3] This method is however limited to specific samples, since non-birefringent material does not lead to any contrast.

### 2.2. *Modern linear methods*

Most modern linear imaging methods usually rely on the specific properties of newly developed light sources, such as long coherence and/or high power, or more sensitive detectors, leading in a general sense to linear scattering microscopy.[4]

In the context of transmission microscopy, most of the developments aim at improving the sensitivity and specificity of the information retrieved from weakly absorbing specimens, by for instance retrieving quantitative values, or improve the image contrast. One approach in this direction consists in quantitative phase microscopy (QPM), for which contrast relies on refractive index values. Several approaches were developed, involving either coherent,[5,6] partially coherent[7–9] or incoherent[10–12] light. QPM is typically a full-field imaging technique which does not involve optical sectioning, although recent advances led to three-dimensional (3D) imaging with these approaches.[13–15] The technique recently found various applications in cell biology where its quantitative aspect led to the derivation of biologically relevant indicators.

Reflectance measurements also gained a wide interest in the past decades, in particular for tissue imaging, thanks to the development of several approaches to locate the depth of the measured information. Reflectance measurements typically have a contrast based on high refractive index differences, which induce strong backscattering. The most noteworthy approach is optical coherence tomography (OCT), which provides optical sectioning through the coherence gating of wide-band sources,[16–19] enabling label-free tomography of tissues, with typical penetration depths in the millimeter range. While OCT has been relatively slow in its original implementation, Fourier domain OCT was shown to have high sensitivity while enabling faster acquisition times by reducing the scanning requirements.[20] Its capability of measuring the intrinsic 3D structure of tissue made this technique an ideal candidate for clinical applications, such as observation of epithelium tissue, or ophthalmologic applications with retina observation. Recent advances have also led to sufficient resolution for cell imaging,[21,22] leading to optical coherence microscopy (OCM). Other more specialized approaches, such as interference reflection microscopy, are based on the interference of reflections at multiple interfaces for studying cell membrane adhesion.[23,24]

### 2.3. *Spectroscopic methods*

Most interactions between light and a sample depend on the wavelength. By spectrally separating scattered or transmitted light, we can often determine detailed information regarding the sample composition. Vibrational bonds in the sample can impart a signature change in the spectrum of incoming light, and by spectral analysis we gain the possibility to analyze the molecular compositions in the sample, which is now becoming possible due to advances in imaging technology. With vibrational energies outside the visible region, molecular composition can be directly probed using infrared or near-infrared wavelengths or instead by looking for the shift in scattered light spectra from vibrational resonances that underlie the process of Raman scattering.[25] Due to the high resolution and chemical

J. Innov. Opt. Health Sci. 2014.07. Downloaded from www.worldscientific.com
by 103.240.126.9 on 10/21/18. Re-use and distribution is strictly not permitted, except for Open Access articles.

specificity, we focus here more on the Raman modality than IR-based or other modes, which usually do not possess resolutions for detailed imaging of cellular structures. With the inherent weakness of the signal in the Raman imaging mode, stemming from the low probability of Raman shifted scattered photons, a number of approaches have been proposed to boost the signals or increase specificity by using either Raman tags[26] or nanoparticles.[27,28]

However, even with the inherent technical difficulties from low signal levels, Raman imaging where the entire spectra is captured (known as spontaneous Raman imaging) is capable of classifying cell types,[29] locating regions of activity in a cell[30] and determining the dynamic changes in molecular distribution in a living cell without labeling.[31,32] In practice, a subset of molecules in the sample exhibit some overlap between the incident light photon energy and the electronic excitation states of the molecule. This leads to "resonant" Raman scattering and boosts the detection sensitivity of Raman imaging for these molecules.[33] This allows more refined measurements of some molecules such as heme-based cytochrome c, which can be tracked and additionally have the redox state mapped during important cellular transitions, such as apoptosis.[34] This is illustrated in Fig. 1, where the heme-based compounds (predominantly located in cytochrome c in mitochondria) in macrophages is contrasted with the lipid distribution, enabling the localization of the two compounds within cells purely by intrinsic molecular contrast. Resonance Raman also allows important diagnostics such as poison toxicity[35] and the progression of malaria parasite infection.[36,37] With Raman imaging still in its relatively early stages, technical advances in signal detection and processing are likely to make this mode more and more useful over the next decade and beyond.

### 2.4. *Nonlinear methods*

Nonlinear imaging methods emerged through the development of high-power pulsed laser sources, which are necessary to compress the laser power to the high peak levels required to generate a nonlinear response. The most well-known imaging application based on nonlinear phenomena is two-photon excited fluorescence (TPEF),[38] where the excitation is performed with high power at twice the usual excitation wavelength to generate fluorescence emission. Nonlinear label-free imaging is also performed

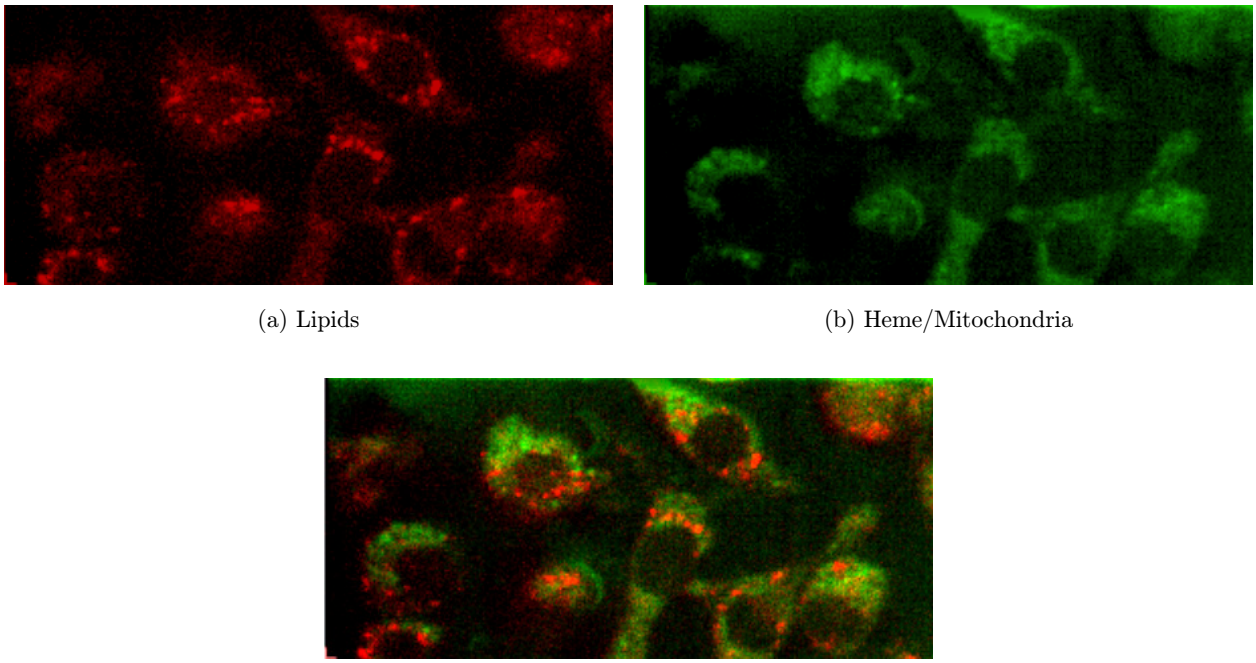

(a) Lipids

(b) Heme/Mitochondria

(c) Overlay

Fig. 1. Label-free Raman imaging of living macrophage MH-S cells, showing two observable components. (a) Lipid band (2850–2870 $cm^{-1}$), (b) Heme band (752-758 $cm^{-1}$), (c) Overlay of both channels.

J. Innov. Opt. Health Sci. 2014.07. Downloaded from www.worldscientific.com
by 103.240.126.9 on 10/21/18. Re-use and distribution is strictly not permitted, except for Open Access articles.

by generating signals such as second harmonic (SHG) or third harmonic (THG), depending on the symmetry of the target molecules. Due to their coherent nature, these signals are typically stronger in transmission, although some backscattered signal also exists, along with depolarization and decoherence of the signal when measured in depth.[39] They usually produce background-free images because of the specific requirements for the sample to generate a significant nonlinear response. Nonlinear imaging is also characterized by an intrinsic sectioning capability, since a nonlinear response occurs only where the light is tightly focused. These properties however impose strict requirements on the light source itself, primarily to ensure that the sufficient compression of the photon density is reached, both spatially and temporally.[40]

For applying SHG in imaging, only noncentrosymmetric materials such as collagen[41,42] or microtubules[43] provide a response, although the molecular source of the SHG contrast is not always clearly known.[44,45] THG does not share the same intrinsic constraints on materials asymmetry, but due to phase-matching requirements, it usually appears at interfaces.[46–48] The technique is used for instance to detect lipids in cells,[49] image full embryos[50] or observe brain tissue.[51]

In addition to coherent processes such as SHG and THG, nonlinear microscopy also enables multiphoton excitation even in the absence of dyes, through two-photon autofluorescence (TPAF).[52] Based on a nonlinear process, this approach also enables 3D imaging, and certain spectral parts of the autofluorescence response can be linked with localized molecules.[53,54] Nonlinear imaging methods present the advantage of high resolution through their excitation scheme, while enabling higher depth penetration of the excitation laser which is located at a higher wavelength. These combined features make them valuable for both cell imaging at high resolution and for tissue imaging, where each technique strives to image deeper in the sample.

## 2.5. *Nonlinear spectroscopic methods*

The development of high-power pulsed lasers also enabled the addition of spectroscopically resolved measurements to the nonlinear processes mentioned above. These techniques utilize the molecular vibrations in a biological sample to generate the image contrast, which can also provide chemical information about the sample.

The two most common nonlinear spectroscopy imaging methods are coherent anti-Stokes Raman scattering (CARS) microscopy and stimulated Raman scattering (SRS) microscopy. Both methods utilize precise excitation beam conditions: usually two laser beams with different optical frequencies excite molecules in a sample to a given vibrational excitation state.[55,56] CARS microscopy detects anti-Stokes scattering light induced by excitation of the molecular vibration, highlighting specific molecular bonds in the sample. SRS microscopy instead uses the energy transfer between the two laser beams, which occurs in the presence of a resonant molecular vibration in the sample. In biological samples, the vibration of $CH_2$ and $CH_3$ is usually the optimum choice for providing contrast in CARS/SRS images, and these are typically assigned to lipids and proteins, respectively.[57] An example of typical contrast is shown in Fig. 2 for both CARS and SRS imaging, displaying high contrast images in both lipids and protein regions.

Compared to spontaneous Raman scattering outlined in Sec. 2.3, CARS and SRS can produce strong signals, allowing rapid imaging of biological samples, with video-rate imaging even demonstrated for observing living cells and tissues.[58,59] The application of CARS and SRS microscopy ranges from cell components like lipid vesicles to tissue diagnosis like brain tissues. While having significant advantages over spontaneous Raman in terms to signal-to-noise, both CARS and SRS are subject to limitations on spectral range and resolution and a further complication for both is the existence of background signals unrelated to molecular vibrations. In CARS microscopy, the background signal comes from nonresonant four-wave mixing contributing to the excitation of the molecular vibration with a resulting drop in image contrast. In SRS microscopy, self-phase modulation and inherent noise from the laser system affect the image contrast. These factors make it difficult in practice to detect low concentrations of molecules by CARS and SRS microscopy.

Practically, Raman imaging is implemented as one of the three above modes (spontaneous, CARS or SRS). Even with an understanding of the physical differences as outlined above, it is not trivial to determine which Raman modality provides the most useful information for a given sample. Due

J. Innov. Opt. Health Sci. 2014.07. Downloaded from www.worldscientific.com
by 103.240.126.9 on 10/21/18. Re-use and distribution is strictly not permitted, except for Open Access articles.

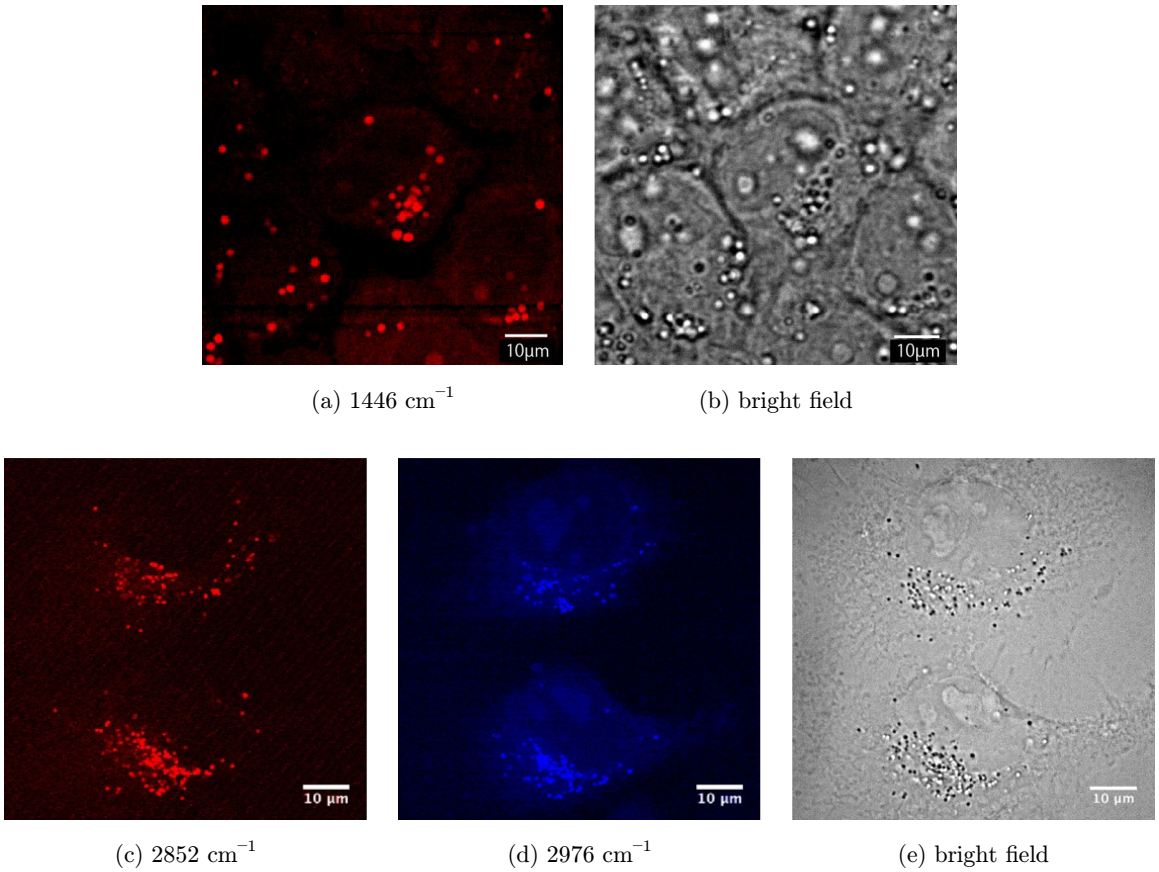


(a) 1446 $cm^{-1}$ (b) bright field

(c) 2852 $cm^{-1}$ (d) 2976 $cm^{-1}$ (e) bright field

Fig. 2. (a) CARS and (c) and (d) SRS imaging at two frequencies on HeLa cells, where each image is compared with a bright field (b) and (e) image taken separately. The red contrast shows lipid structures, while the blue contrast represents proteins.

to their high signal to noise and rapid imaging capability, CARS and SRS are becoming popular and provide label-free images of a number of different samples with the image contrast based on known vibrational bands. Spontaneous Raman imaging scattering is usually weaker than CARS or SRS, but as a trade-off provides the full spectrum of Raman active vibrations of the molecules in the sample with higher resolution. Spontaneous Raman imaging is therefore usually slower but contains data richer in molecular information compared to CARS or SRS, where even with recent advances it is challenging to take a wide range of spectra with high spectral resolution.

Sum frequency generation (SFG) microscopy has also been applied to image and analyze materials at surfaces.[60–62] In SFG microscopy, infrared laser light and visible wavelengths are incident on a sample. SFG is strongly induced when the sample absorbs the incident IR light, and can be used to investigate the sample molecules. Since SFG (like SHG mentioned above) is a second-order nonlinear optical effect, interfaces or non-centrosymmetric structures in the sample are the main targets of the observation.

## 2.6. *Hybrid methods*

In addition to the purely optical methods presented in the sections above, recent developments showed the utility of hybrid methods, where the excitation/detection is not performed purely by optical means. In particular, photoacoustic microscopy (PAM) emerged as a promising method for deep tissue imaging.[63,64] This approach relies on the transient mechanical strain which appears through the tissue dilation induced by the absorption of light, which is then detected as ultrasound waves. Through proper tomographic reconstruction algorithms, this measurement can lead to three-dimensional images, whereas the hybrid measurement approach can provide deeper penetration in tissue.[65]

Even though the original feature of merit in PAM was its high penetration depth, imaging at

J. Innov. Opt. Health Sci. 2014.07. Downloaded from www.worldscientific.com by 103.240.126.9 on 10/21/18. Re-use and distribution is strictly not permitted, except for Open Access articles.

cellular resolution has also been demonstrated by employing high-aperture optics, both in transmission[66] and reflection.[67] By employing an excitation wavelength in a suitable absorption range, this approach could be used to image cell nuclei[68] or cytochromes.[69] Similarly, measuring a chosen range of acoustic frequencies can for example provide information about cell morphologies.[70]

The heating effects of the excitation light can also be measured through photothermal imaging, which detects the local modifications of the refractive index.[71] While this approach has often beem used with nanoparticles to enhance the heating effects,[72] measurement have also been applied to living organisms[73] and cells, making it possible for example to image mitochondria[74] or intracellular heme.[75]

### 2.7. *Technical aspects of combining label-free modes*

To enable multimodal imaging, we need to be able to record several types of images, which can require very different hardware components for each mode, making the whole multimodal setup overly complex. However, certain modes share some similarities in setup requirements. Several recently developed microscopy techniques such as nonlinear methods in Secs. 2.4 and 2.5 are based on similar physical principles. They then rely on laser-scanning schemes, with high peak power excitation, and sensitive detectors, such as photo-multiplier tubes (PMT). Nonlinear spectroscopic methods also require adjustable laser sources, such as optical parametric oscillators (OPO).

On the other hand, modes based on spectroscopy (see Sec. 2.3) typically involve narrow excitation lines and wide-band spectrally resolved detection, thus limiting the excitation light sources, and generally require spatially resolved detectors (line or two-dimensional) to enable spectral measurements. Multimodal Raman implementations have, for example, been limited by the requirement to allocate nearly the entire emission wavelength range to the spectroscopic detection.

Finally, OCT relies on wide-band sources, since the spectral width determines the resolution along the optical axis, so that sources such as superluminescent diodes (SLD) or temporally compressed pulses are usually employed. On the contrary, QPM relies on narrow sources with sufficient coherence to generate interferograms, or relies on specific detectors or actuators.

Aside from allocating spectral or wavelength ranges for each mode, the physical layout of the setup can make multimodal implementation difficult. The majority of recent microscopy techniques rely on epi-detection schemes, which simplifies the suppression of background light. However, some coherent techniques such as QPM are based on transmission, and nonlinear coherent processes such as SHG and THG can be detected in either direction but exhibit a stronger signal in the forward direction.

Together, these aspects imply that while some imaging modes can be combined using similar hardware and measurement procedures, the fact of combining others requires significantly extending the hardware of the setup, due to major technical differences.

### 2.8. *Signal separation approaches*

Multimodal label-free imaging can be challenging, as there is a need to separate the information retrieved from the various modes. Without using a specific contrast agent with a known optical response, the separation can be performed only by exploiting either specific features of the illumination source itself, or by using known properties of the intrinsic optical response for a given mode.

In practice, the main optical properties which we can exploit to separate modal information are the wavelength and polarization or other coherence properties of the emitted light. Spectrally narrow band modes can be readily separated by edge or bandpass filters if the modal spectra do not overlap. This approach then works well when the spectral responses are known and non-overlapping, for example harmonic generation or the selection of a resonant band in nonlinear spectroscopy.

Similarly, orthogonal polarizations can easily be separated by employing polarizing optics, to either separate or recombine polarization states to image optical responses which preserve polarization, or to generate specific excitation patterns for polarization-dependent phenomena.

Other separation schemes are based on the modulation of the signal, in order to separate a signal bandwidth from another. The modulation can be performed in the spatial domain, which is suitable for techniques employing coherent detection, or in the temporal domain, where the excitation source is modulated.

The separation approaches described here imply that white light-based methods are generally not

J. Innov. Opt. Health Sci. 2014.07. Downloaded from www.worldscientific.com by 103.240.126.9 on 10/21/18. Re-use and distribution is strictly not permitted, except for Open Access articles.

suitable for simultaneous multimodal imaging, as they are usually unpolarized with a wide spectral bandwidth, so that it is usually complicated to separate other signals from white light-based methods.

## 3. Multimodal Label-Free Imaging

A large amount of multimodal applications have been developed in the various fields covered in this review, where the different possibilities provide numerous possible combinations. A summary of the various applications can be found in Table 1, in which the various reports are classified in order to show the different multimodal applications which have been achieved. A simple list of combinations without redundancy would only require half of the table. However, even the claim that two modes have been combined can be an oversimplification. Some reports use two complete independent and simultaneous modes, and some instead combine the measurement concepts of two modes, generating a signal on its own. We therefore separated the table into each one half where the implementation uses independent modes (lower-left table, "Combined multimodal") or by combining measurement principles (upper-right table, "Combined concept").

As examples, where for instance an OCT-like signal is measured from the SHG would be listed as conceptual multimodal, while an experiment where SHG and CARS signals are measured independently would be listed in the combined multimodal section. Reports are further classified into one of the following categories: not done; done but not simultaneous; simultaneous; and well-established. These designations are meant to be organizational and not a judgment on the value of the work.

In addition to the modes described in Sec. 2, the table also contains a line for polarization-resolved measurements, where each mode can possibly be extended to measure various polarization states. Furthermore, we also added another mode, denoted as absorption spectroscopy (AS). While this approach has not been discussed previously since it is usually not used for imaging purposes, we employ this

Table 1. Overview of current state of multimodal implementations. The table aims to show which modes have to date been combined and to what degree the multimodal combination was successful. The lower-left region of the table shows where the two modes were combined using simultaneous and independent measurement of both modes information. The upper-right part of the table shows where the two modes are multimodal in concept but do not provide two separate modes independently.

| Combined concept | | | | | | | | | | |
|---|---|---|---|---|---|---|---|---|---|---|
| | QPM | OCT | AS | Raman | SHG | THG | TPAF | CARS | SRS | PAM |
| Pol. | ◎[88,89] | ◎[93,95] | × | ◊[109] | ◎[42,83] | □[84,85] | × | □[144] | × | × |
| QPM | | × | ◊[132] □[131] | × | □[76,99,194] | × | × | □[146] | × | × |
| OCT | × | | ◎[4] | × | □[103] | × | × | □[149] | × | × |
| AS | × | × | | × | × | × | □[53,54] | × | × | ◎[167,168] |
| Raman | ◊[125] □[126] | □[117] | × | | × | × | × | × | × | × |
| SHG | × | □[101,105,106] | × | □[112] | | × | × | × | × | × |
| THG | × | × | × | × | ◎[49,50] | | × | × | × | × |
| TPAF | × | □[102,175] | × | □[178] | ◎[45] | ◎[49] | | × | × | □[169] |
| CARS | □[147,148] | × | × | ◊[162,163] | ◎[137] | ◎[143] | ◎[77] | | × | × |
| SRS | × | × | × | × | × | × | × | × | | □[170,171] |
| PAM | × | □[164,165] | × | × | × | × | × | × | × | |
| Combined multimodal | | | | | | | | | | |

*Notes*: × not done, ◊ not simultaneous, □ simultaneous, ◎ well established.
Pol.: polarization, QPM: quantitative phase microscopy, OCT: optical coherence tomography, AS: absorption spectroscopy, SHG: second-harmonic generation, THG: third-harmonic generation, TPAF: two-photon autofluorescence, CARS: coherent anti-Stokes Raman spectroscopy, SRS: stimulated Raman spectroscopy, PAM: photoacoustic microscopy.

J. Innov. Opt. Health Sci. 2014.07. Downloaded from www.worldscientific.com by 103.240.126.9 on 10/21/18. Re-use and distribution is strictly not permitted, except for Open Access articles.

denomination to classify imaging modes which have been extended to spectrally resolved measurements.

### 3.1. *Nonlinear multimodal implementations*

Multimodal applications based on different nonlinear phenomena are presented first. One of the most established label-free multimodal implementations, possess several characteristics making them ideal for multimodal use. The same optical configuration can often lead to multiple nonlinear effects, such as simultaneous SHG, THG and TPAF, which are located at different wavelength ranges in the optical spectrum, making them easy to filter. In particular, when the measurement configuration allows for more demanding modes such as THG, which requires higher temporal compression, other nonlinear signals such as SHG or TPAF are also emitted and can be readily measured. With a large number of applications already established, performing an exhaustive review of all applications is beyond the scope of this article. Fortunately, several reviews already adequately cover this field.[45,77]

In addition to these combinations which have been well established in the past years, more specific use has also been made of multimodal nonlinear responses, such as combining several harmonics of autofluorescence,[78] characterizing cell types such as cancerous cells through their nonlinear responses,[79] differentiating several tissue types in mucosa[80] or performing *in vivo* imaging of complete small organisms.[50,81,82]

Due to the coherent state of the harmonic generation, polarization-resolved measurements are also possible, and work well in particular for SHG, where the non-symmetric requirements makes it very sensitive to the polarization state of the excitation beam.[42,83] Due to its strong sensitivity to local molecular arrangement, the intensity of THG is also dependent on the incoming polarization, which can be used to probe crystal orientations[84] or assess lipid orientation in cells.[85]

### 3.2. *Linear multimodal implementations*

Linear microscopy methods have not often been combined with other linear methods, as the main modes in this category all possess rather different technological requirements and measurement approaches, making it not trivial to combine them, for example transmission by QPM and back-scattering measurement by OCT.

Within linear imaging, QPM has been combined with confocal reflectance, making it possible to estimate the cell size and solve the ambiguity of QPM between cell height and refractive index.[86] QPM has also been simultaneously combined with incoherent imaging (bright field microscopy or autofluorescence) by employing the spatial modulation properties of QPM.[87]

Several applications enabling polarization-resolved measurement with QPM have been reported. QPM is well suited to this combination due to the possibility of selecting the measured polarization through the state of the reference beam. Simultaneous extraction of the polarization information has been performed either through spatial modulation,[88,89] or with microarrays.[90] More complicated implementations can even allow the extraction of all Stokes parameters instead of two orthogonal polarization states.[91]

In the case of OCT, the coherent tomography principle has been combined with dark-field illumination to enhance the image contrast of cell preparations.[92] Polarization-resolved OCT has also been reported, fully characterizing the polarization state of the backscattered beam,[93–95] or used to measure the birefringence of the sample at high speed.[96]

Due to the coherent nature of the detection of imaging modes such as QPM and OCT, several applications have been reported to combine coherent processes such as SHG and interferometric approaches. Combined SHG-QPM was first reported for nanocrystals,[97] before being applied to polarization-resolved measurements,[98,99] and biological specimens.[76,100] Figure 3 shows an example of the coherent detection of the SHG emitted by a mouse tail section, where it is possible to identify the enhanced SHG signal in amplitude due to coherent detection, along with its corresponding phase information.

Similarly, OCT has been combined with SHG measurements,[101,102] and the first SH-OCT measurements have been reported on collagen layers[103] and rat tendon.[104] Multimodal imaging of both fundamental and SH-OCT were later reported for various types of tissue.[105,106] Due to their sensitivity to tissue structures, and being label-free, this type of multimodal imaging is likely to become increasingly clinically relevant in the future.

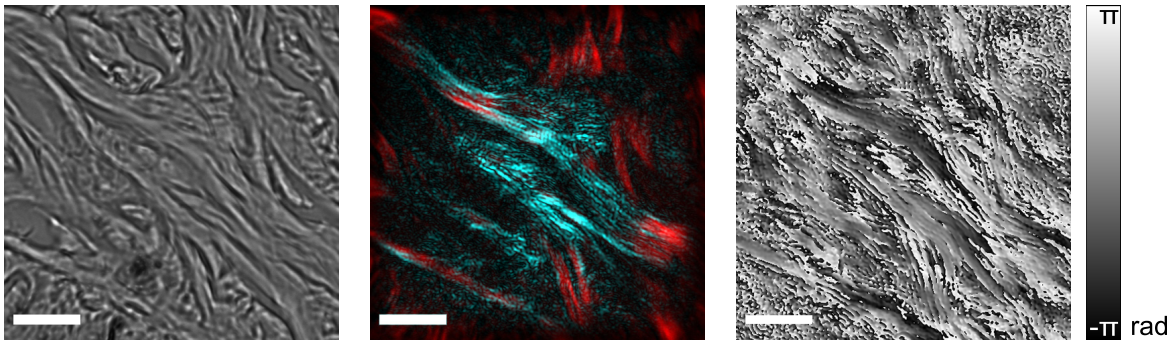


(a) (b) (c)

Fig. 3. Mouse tail dermis and epidermis. (a) Bright field image, (b) Overlay of (red) cross-polarization image showing phase retardation caused by the birefringence of collagen and (blue) SHG amplitude (normalized), (c) phase (wrapped) reconstructed from a single hologram. All images present the same region of the specimen and scale bars are 10 $\mu$m. Adapted with permission from Ref. 76.

### 3.3. *Spectroscopic multimodal implementations*

Spectroscopic imaging possesses features that make it not trivial to implement in multimodal applications. The wide wavelength range complicates spectral filtering, and often, low-intensity signals (especially in vibrational spectroscopy) can prevent the simultaneous measurement with other modes which would swamp the vibrational response signal. Raman imaging was for example recently combined with autofluorescence in sequential measurements to accelerate the detection of tumors by combining the faster but less specific fluorescence with the slower but highly specific spectroscopic signal.[107]

Polarization-resolved Raman is known to provide selectivity in the vibrational response with molecular orientation, such as for DNA molecules.[108] This approach has been recently implemented in an imaging mode[109] to enhance selected chemical responses or to attain z-resolved polarization measurements.[110] The Raman scattering process itself can be generated by two-photon processes[111] although it is generally much easier to implement with the use of nanostructures[112] or by the addition of nanoparticles to generate surface-enhanced Raman scattering (SERS).[113,114]

Due to their similar measurement configurations (laser scanning with detection of backscattered light), Raman and OCT have been combined in order to retrieve both the 3D structure and the vibrational spectrum, either with point-measurements in Raman,[115,116] or with imaging in both modalities through sample scanning.[117]

As OCT employs wide-band light sources to generate optical sectioning, an extension denoted as spectral OCT (S-OCT) consists in resolving spectrally the measurement to obtain both the 3D structure through OCT, as well as the absorption spectra.[4,118] This approach has been reported for both temporal[119] and Fourier domain[120,121] S-OCT, leading to different performances,[122] which are also dependent on the employed compensation procedures.[123] The spectroscopic measurement can typically lead to various invaluable information such as blood oxygenation.[124]

Despite their fundamental differences in imaging principle, Raman has also been combined with QPM. This has been performed either through successive measurements (i.e., not simultaneous),[125] or by employing a narrow spectrum source outside the Raman response for simultaneous measurements.[126] This is illustrated in Fig. 4, where simultaneous QPM and Raman of live cells enable the comparison of the elastic scattering along with the inelastic vibrational spectra. The combination of the two modes allows the Raman chemical information to determine which molecules contribute to the phase signal, while the phase information can track how the cell is changing during the slower Raman image acquisition and compensate for motion blur.

Spectroscopic applications are not extensive in QPM, but some reports studied applications with 2–3 discrete wavelengths,[127,128] allowing for example intracellular refractive measurements based on dispersion,[129] or quantification of hemoglobin concentration.[130] More recently, full spectroscopic measurements have been achieved in QPM on samples on reflective surfaces in a configuration similar to S-OCT,[131] or by employing a sweeping source.[132]



J. Innov. Opt. Health Sci. 2014.07. Downloaded from www.worldscientific.com by 103.240.126.9 on 10/21/18. Re-use and distribution is strictly not permitted, except for Open Access articles.

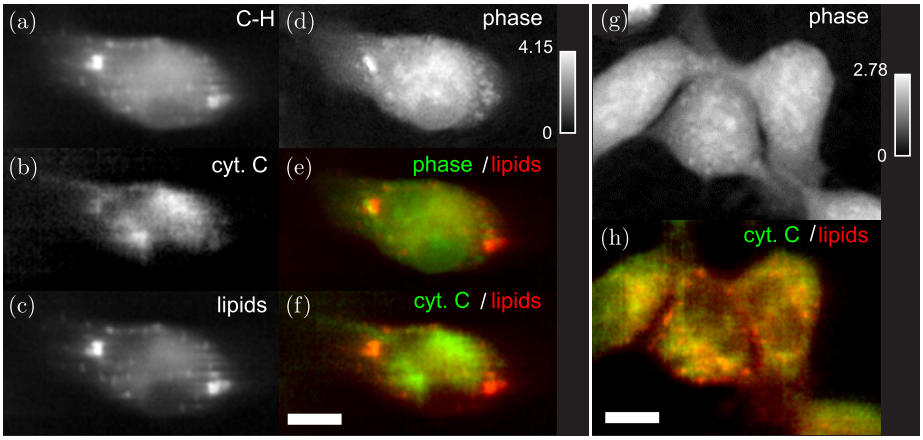


Fig. 4. Simultaneous QPM and Raman measurements on MH-S macrophage (a)–(f) and HeLa (g) and (h) cells. The source of image contrast are (a) c–h stretching band (2935–2955 $cm^{-1}$), (b) cytochrome C band (740–780 $cm^{-1}$), (c) lipid band (2860–2880 $cm^{-1}$), (d) and (g) phase, (e), (f), (h) Overlay images. The phase dynamic range is given in radians, and scale bars are 5 $\mu$m.

### 3.4. *Nonlinear spectroscopy multimodal implementations*

Compared to linear spectroscopy, nonlinear techniques such as CARS are easier to combine with other modes, as the spectral range they utilize is usually smaller. In particular, since the laser source required for nonlinear spectroscopy is similar to the sources used for the other one of nonlinear processes mentioned above, many different combinations are available, and CARS has been extensively combined with phenomena such as SHG, THG or TPAF.[77,133] CARS-SHG has been used for several different samples, such as *Caenorhabditis Elegans*,[134] the central nervous system,[135] or skin,[136] as shown for example in Fig. 5 where CARS and SHG have been measured simultaneously on cardiomyocyte cells. CARS has also been used along with TPAF for skin imaging[137,138] or small organism imaging.[139] As several excitation sources are required for CARS, other nonlinear frequencies such as SFG can be implemented directly, and possibly simultaneously.[140] Similarly, comparative imaging of collagen with SFG and SHG has been shown.[141] When employing several nonlinear combinations, the measurement of up to four simultaneous modes could be demonstrated,[142,143] opening new possibilities for the derivation of complementary information from each independent mode.

Polarization-resolved CARS could also be performed,[144] as well as interferometric detection of CARS,[145,146] both leading to background-free signals, thus overcoming one of the main drawbacks of this technique. Combining CARS and interferometric detection also led to holographic CARS imaging.[147,148] Recent reports also demonstrated the capability of detecting backscattered CARS signals with OCT configurations.[149]

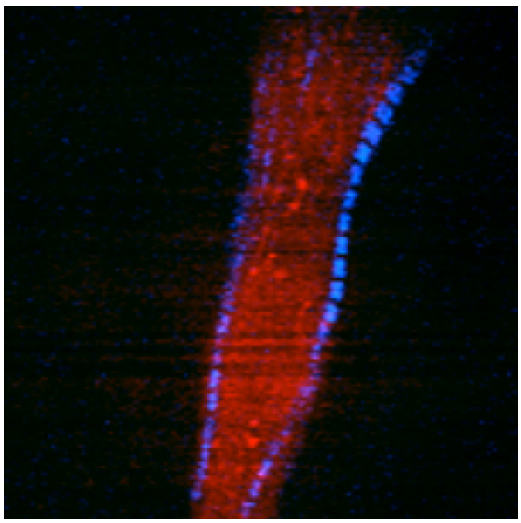

Fig. 5. Simultaneous SHG (blue) and CARS (red, 1446 $cm^{-1}$) signals measured on cardiomyocyte cells, displaying the membrane of the cell and its inner structure (respectively).

By employing broadband sources, spectral windows have been observed with CARS,[150] leading to enhanced vibrational spectroscopy over a limited spectral band in cells[151] and tissues.[152] Some applications also report wide-band spectral imaging with multiplexed CARS, at some cost in signal-to-noise.[153,154] Multiplexed SRS was also demonstrated recently, either by rapidly sweeping the pump excitation,[155,156] or by multiplexing different frequencies temporally.[157] On the other hand, the

J. Innov. Opt. Health Sci. 2014.07. Downloaded from www.worldscientific.com by 103.240.126.9 on 10/21/18. Re-use and distribution is strictly not permitted, except for Open Access articles.

J. Innov. Opt. Health Sci. 2014.07. Downloaded from www.worldscientific.com by 103.240.126.9 on 10/21/18. Re-use and distribution is strictly not permitted, except for Open Access articles.

combination of SRS with other modalities has not yet been reported to our knowledge, as the measurement scheme of SRS is based on temporal modulation, which makes it less ideal for combination with other methods employing constant intensity.

Linear and nonlinear Raman spectroscopy have been compared in several reports,[158,159] but due to the large difference in measurement principle, and that both modalities probe similar vibrations, no simultaneous measurements were performed. Additionally, most applications employ CARS as an imaging technique, while until recently, Raman was nearly always implemented as a nonimaging spectroscopy technique measured at one point.[160,161] Some recent reports present measurements performed sequentially on the same samples, either on brain slices[162] or on fixed cells.[163]

### 3.5. *Hybrid methods*

The measurement approach of PAM, ideal for tissue imaging, makes it very convenient for combination with OCT, in order to retrieve two types of contrasts (scattering and absorption) resolved in depth.[164] The combination could be made simpler by employing the same excitation source for both OCT and PAM.[165] A similar approach could be employed to demonstrate the combination of PAM with reflection confocal microscopy for live cell measurements.[166]

As the source of contrast of PAM is based on absorption, its extension to spectroscopic measurement is straightforward by spanning the wavelength of the excitation source, leading to functional imaging to measure for example the oxygen saturation in blood vessels, water concentration, or DNA and lipids in cells.[167,168]

The detection principle of PAM could also be used with nonlinear optical processes such as two-photon absorption for high spatial resolution.[169] The combination of PAM with nonlinear effects such as SHG/THG is however not directly possible as these methods are based on a coherent generation of a secondary optical signal. Vibrational modes could also be measured with PAM by employing stimulated Raman excitation, leading to *in vivo* molecular contrast.[170,171]

## 4. Recent Developments in Combination with Labeled Modes

While this review focuses on label-free modalities, labeled imaging has of course had an enormous impact on the field of microscopy and driven many important discoveries in biology and other fields. With the extensive use of contrast agents, label-free modalities have also been coupled with the use of dyes, and in particular fluorescent labels. This section aims at briefly mentioning the main application trends in which this type of coupling is applied, without claiming to be exhaustive. For some of these particular applications, the coupling between label-free methods and contrast agents brings new opportunities.

Linear methods have been coupled with fluorescence, essentially with the aim of adding functional information to the existing imaging mode. QPM has been used with linear fluorescence either sequentially,[172] or simultaneously with spectral[173] or spatial[87] filtering schemes. For OCT, laser scanning aimed mainly for tissue, the measurement approach makes it less suitable for coupling with linear fluorescence, although applications have been shown successful with pump-probe approaches.[174] OCT is, however, ideal for coupling with TPEF, where the same source can be used for both modalities.[175–177]

Spectroscopic methods such as Raman imaging are not easily coupled to fluorescence, due to their wide band and weak signal which makes the separation complicated. For this reason, most applications measure the two modalities sequentially, staining the sample after having already measured the Raman spectrum.[31] This approach is feasible but clearly allows only one chance to obtain the Raman measurement and multimodal tracking of a cell response would not be possible. Simultaneous measurement could also be demonstrated with TPEF, where the fluorescence is situated at higher energy than the Raman scattering.[178,179]

Nonlinear methods and spectroscopic ones such as CARS have been extensively used with TPEF, thanks to their similar measurement protocols.[45,77,180,181] These approaches have also been combined with light sheet microscopy[82] or fluorescence lifetime imaging.[182]

In addition to fluorescent tags, label-free approaches have been coupled to contrast agents such as nanocrystals or nanoparticles,[183] especially for SERS measurements.[184]

Fluorescence imaging is the collection of inherently incoherent emission, and resolving the fluorophores along the optical axis requires specific measurement schemes, such as confocal microscopy,[185] or nonlinear excitation with TPEF. Another approach based on

J. Innov. Opt. Health Sci. 2014.07. Downloaded from www.worldscientific.com
by 103.240.126.9 on 10/21/18. Re-use and distribution is strictly not permitted, except for Open Access articles.

coherent detection of the fluorescent emission has also been proposed recently, where labels can be located in 3D through the estimation of their phase. This approach has been reported with optical scanning holography (OSH), where an interferometric pattern is generated in the object plane with specimen scanning,[186,187] or through self-reference, either in the time or Fourier domain.[188] Another approach, fluorescence incoherent color holography (FINCH), employs an inline interferometric scheme coupled to phase-shifting methods to enable full-field 3D acquisition of fluorescence without needing to scan the object.[189,190]

While Raman spectroscopy presents several challenges for being coupled with fluorescence imaging, it was demonstrated recently that specific tags can be employed to enable simultaneous Raman microspectroscopy along with functional labels measurement by the creation of specific Raman tags which vibrationally resonate within the Raman silent region, thus being spectrally independent of the spectroscopic measurement.[26,191] An example of this principle is shown in Fig. 6, where live HeLa cells have been loaded with an alkyne molecule as a contrast agent, which gradually accumulates in the cell nuclei.

SHG is mainly a label-free imaging modality, whose contrast originates from non-centrosymmetric materials such as collagen or fibers. However, if an SHG-active material is introduced into a sample,

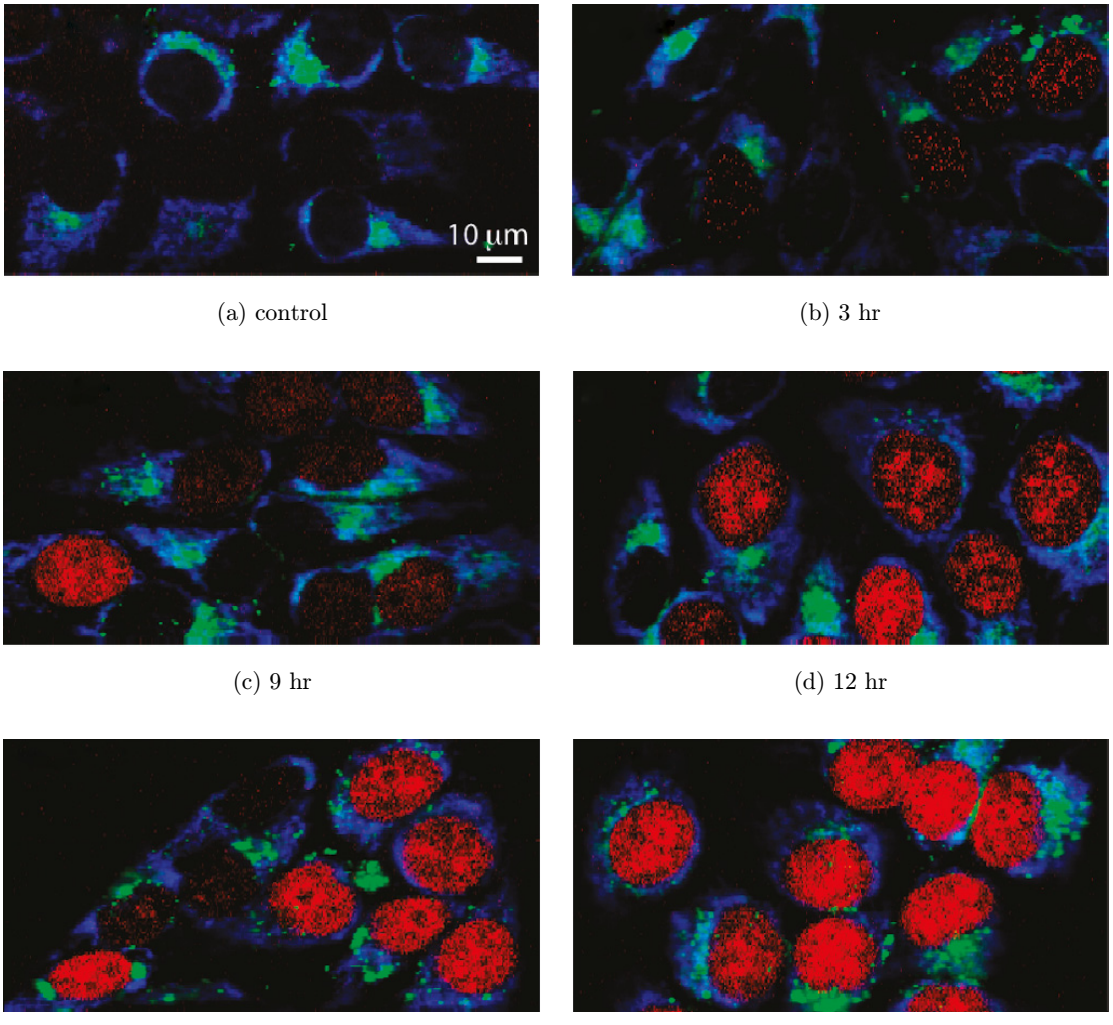


(a) control (b) 3 hr

(c) 9 hr (d) 12 hr

(e) 14 hr (f) 21 hr

Fig. 6. Time-course Raman images of HeLa cells cultured with alkyne labels, which emit in the Raman silent region (2123 $cm^{-1}$). The overlay was constructed with 749, 2123 and 2849 $cm^{-1}$ bands, shown respectively as blue, red and green. Reprinted with permission from Ref. 26. Copyright (2011) American Chemical Society.

J. Innov. Opt. Health Sci. 2014.07. Downloaded from www.worldscientific.com
by 103.240.126.9 on 10/21/18. Re-use and distribution is strictly not permitted, except for Open Access articles.

very strong signals can be retrieved. SHG-active nanocrystals can therefore be exploited and can be accurately located in three-dimensions because of the nonlinearity in the excitation scheme,[192] providing a signal strong enough to be detectable within living tissue.[193] These labels were in particular used with coherent detection of SHG to enable highly resolved imaging in turbid media such as tissue,[194] where the nanocrystals are used as references to compensate for the inherent scattering of the specimen.[195,196]

The observation of fluorescent labels in nonlinear regimes is usually performed through TPEF, but it could be demonstrated that in particular conditions, SHG can also be employed with significant benefits. In the case of dyes attached to the cell membrane, the symmetry can be locally broken so that a spatially selective signal can be measured, contrarily to TPEF which is emitted by the whole cell.[197] Additionally, it is possible to linearly relate the SHG intensity emitted by the dyes to the membrane potential.[198] This approach therefore provides a pure optical means of measuring the membrane potential of excitable cells such as myocytes or neurons,[199] with several choices of dyes,[200] which is of great interest to cell biologists.

## 5. Conclusion

This paper reviewed the current state of the field for label-free multimodal imaging. As stated, combining label-free methods ranges from simple to highly complex, depending on the type of modes to be combined. The complexity results from attempting to combine modes which rely on very different physical interactions and/or compete for spectral bandwidth, but it is often precisely these combinations which provide the most useful information. Label-free imaging itself is increasingly being recognized as a challenging but worthwhile endeavour. The advantages of label-free imaging go beyond the obvious fact that it does not modify the sample; the retrieved signal originates directly from the observed specimen without requiring any assumption of which additional tags should be inserted, as in case of label-based imaging. As an example, by not labeling the sample and instead using Raman imaging we are not forced to make assumptions regarding the expected changes or targets of interest during a reaction in a living cell. Instead, the technical challenge becomes the low amount of emitted signals, even as the emitted information is rich in molecular details.

Several examples described in this review demonstrated the innovative capability of combining label-free modes, such as the multiple contrast which can be obtained in nonlinear imaging, the possibility of overcoming inherent limitations of techniques such as suppressing the background of CARS with an interferometric approach, or the capability of retrieving the information about different physical processes in a simultaneous manner with for example SHG-OCT or QPM/Raman simultaneous capabilities. Even when employing labels, the advantage of employing a label-free approach was shown for instance through the additional specificity of SHG over TPEF when observing cell membranes.

As such, the implementation of simultaneous modes can be an elegant solution to technical issues or biological problems, if done in a manner that does not disturb the original mode (i.e., independently and possibly without labeling). It is also possible, as mentioned, to generate fundamentally new information from the combination of non-redundant and complementary modes. From the comparisons done in this paper, and the attempt to generally categorize the entire field of multimodal implementations, we hope to highlight what might be possible, and to encourage further progress.

## Acknowledgments

The authors would like to thank Dr. E. Shaffer for providing the figures of combined second harmonic and quantitative phase imaging. We acknowledge funding from the Japan Society for the Promotion of Science (JSPS) through the Funding Program for World-Leading Innovative R&D on Science and Technology (FIRST Program), and JSPS World Premier International Research Center Initiative Funding Program.

## References

1. F. Zernike, "How I discovered phase contrast," *Science* **121**, 345–349 (1955).
2. R. Allen, G. David, G. Nomarski, "The Zeiss-Nomarski differential interference equipment for transmitted-light microscopy," *Z. Wiss. Mikrosk.* **69**, 193–221 (1969).

J. Innov. Opt. Health Sci. 2014.07. Downloaded from www.worldscientific.com by 103.240.126.9 on 10/21/18. Re-use and distribution is strictly not permitted, except for Open Access articles.


3. R. Oldenbourg, "A new view on polarization microscopy," *Nature* **381**, 811–812 (1996).
4. N. N. Boustany, S. A. Boppart, V. Backman, "Microscopic imaging and spectroscopy with scattered light," *Annu. Rev. Biomed. Eng.* **12**, 285–314 (2010).
5. E. Cuche, P. Marquet, C. Depeursinge, "Simultaneous amplitude-contrast and quantitative phase-contrast microscopy by numerical reconstruction of Fresnel off-axis holograms," *Appl. Opt.* **38**, 6994–7001 (1999).
6. I. Yamaguchi, J.-I. Kato, S. Ohta, J. Mizuno, "Image formation in phase-shifting digital holography and applications to microscopy," *Appl. Opt.* **40**, 6177–6186 (2001).
7. M. R. Arnison, K. G. Larkin, C. J. R. Sheppard, N. I. Smith, C. J. Cogswell, "Linear phase imaging using differential interference contrast microscopy," *J. Microsc.* **214**, 7–12 (2004).
8. S. Bernet, A. Jesacher, S. Frhapter, C. Maurer, M. Ritsch-Marte, "Quantitative imaging of complex samples by spiral phase contrast microscopy," *Opt. Express* **14**, 3792–3805 (2006).
9. S. S. Kou, L. Waller, G. Barbastathis, C. J. R. Sheppard, "Transport-of-intensity approach to differential interference contrast (TI-DIC) microscopy for quantitative phase imaging," *Opt. Lett.* **35**, 447–449 (2010).
10. N. Streibl, "Phase imaging by the transport equation of intensity," *Opt. Commun.* **49**, 6–10 (1984).
11. A. Barty, K. Nugent, D. Paganin, A. Roberts, "Quantitative optical phase microscopy," *Opt. Lett.* **23**, 817–819 (1998).
12. P. Bon, G. Maucort, B. Wattellier, S. Monneret, "Quadriwave lateral shearing interferometry for quantitative phase microscopy of living cells," *Opt. Express* **17**, 13080–13094 (2009).
13. W. Choi, C. Fang-Yen, K. Badizadegan, S. Oh, N. Lue, R. R. Dasari, M. S. Feld, "Tomographic phase microscopy," *Nat. Methods* **4**, 717–719 (2007).
14. M. Debailleul, V. Georges, B. Simon, R. Morin, O. Haeberlé, "High-resolution three-dimensional tomographic diffractive microscopy of transparent inorganic and biological samples," *Opt. Lett.* **34**, 79–81 (2009).
15. Y. Cotte, F. Toy, P. Jourdain, N. Pavillon, D. Boss, P. Magistretti, P. Marquet and C. Depeursinge, "Marker-free phase nanoscopy," *Nat. Photonics* **7**, 113–117 (2013).
16. D. Huang, E. Swanson, C. Lin, J. Schuman, W. Stinson, W. Chang, M. Hee, T. Flotte, K. Gregory, C. Puliafito, J. G. Fujimoto, "Optical coherence tomography," *Science* **254**, 1178–1181 (1991).
17. J. Schmitt, "Optical coherence tomography (OCT): A review," *IEEE J. Quantum Electron.* **5**, 1205–1215 (1999).
18. M. Wojtkowski, R. Leitgeb, A. Kowalczyk, T. Bajraszewski, A. F. Fercher, "In vivo human retinal imaging by Fourier domain optical coherence tomography," *J. Biomed. Opt.* **7**, 457–463 (2002).
19. A. F. Fercher, W. Drexler, C. K. Hitzenberger, T. Lasser, "Optical coherence tomography — principles and applications," *Rep. Prog. Phys.* **66**, 239–303 (2003).
20. R. Leitgeb, C. Hitzenberger, A. Fercher, "Performance of fourier domain vs. time domain optical coherence tomography," *Opt. Express* **11**, 889–894 (2003).
21. J. A. Izatt, M. D. Kulkarni, H.-W. Wang, K. Kobayashi, M. V. J. Sivak, "Optical coherence tomography and microscopy in gastrointestinal tissues," *IEEE J. Quantum Electron.* **2**, 1017–1028 (1996).
22. A. D. Aguirre, Y. Chen, B. Bryan, H. Mashimo, Q. Huang, J. L. Connolly, J. G. Fujimoto, "Cellular resolution ex vivo imaging of gastrointestinal tissues with optical coherence microscopy," *J. Biomed. Opt.* **15**, 016025 (2010).
23. A. S. G. Curtis, "The mechanism of adhesion of cells to glass: A study by interference reflection microscopy," *J. Cell Biol.* **20**, 199–215 (1964).
24. H. Verschueren, "Interference reflection microscopy in cell biology: Methodology and applications," *J. Cell Sci.* **75**, 279–301 (1985).
25. S. Šašić, Y. Ozaki (Eds.) *Raman, IR, and Near IR Chemical Imaging*, John Wiley & Sons, Inc. (2011).
26. H. Yamakoshi, K. Dodo, M. Okada, J. Ando, A. Palonpon, K. Fujita, S. Kawata, M. Sodeoka, "Imaging of EdU, an alkyne-tagged cell proliferation probe, by raman microscopy," *J. Am. Chem. Soc.* **133**, 6102–6105 (2011).
27. D. A. Stuart, A. J. Haes, C. R. Yonzon, E. M. Hicks, R. P. Van Duyne, "Biological applications of localised surface plasmonic phenomenae," *IET Nanobiotechnol.* **152**, 13–32 (2005).
28. X. Huang, I. H. El-Sayed, W. Qian, M. A. El-Sayed, "Cancer cells assemble and align gold nanorods conjugated to antibodies to produce highly enhanced, sharp, and polarized surface raman spectra: A potential cancer diagnostic marker," *Nano Lett.* **7**, 1591–1597 (2007).
29. J. K. Pijanka, D. Kumar, T. Dale, I. Yousef, G. Parkes, V. Untereiner, Y. Yang, P. Dumas, D. Collins, M. Manfait, G. D. Sockalingum, N. R. Forsyth, J. Sule-Suso, "Vibrational spectroscopy differentiates between multipotent and pluripotent stem cells," *Analyst* **135**, 3126–3132 (2010).

J. Innov. Opt. Health Sci. 2014.07. Downloaded from www.worldscientific.com by 103.240.126.9 on 10/21/18. Re-use and distribution is strictly not permitted, except for Open Access articles.


30. D.-H. Kim, R. Jarvis, J. Allwood, G. Batman, R. Moore, E. Marsden-Edwards, L. Hampson, I. Hampson, R. Goodacre, "Raman chemical mapping reveals site of action of HIV protease inhibitors in HPV16 E6 expressing cervical carcinoma cells," *Anal. Bioanal. Chem.* **398**, 3051–3061 (2010).
31. H.-J. van Manen, Y. M. Kraan, D. Roos, C. Otto, "Single-cell Raman and fluorescence microscopy reveal the association of lipid bodies with phagosomes in leukocytes," *Proc. Natl. Acad. Sci. USA* **102**, 10159–10164 (2005).
32. K. Hamada, K. Fujita, N. I. Smith, M. Kobayashi, Y. Inouye, S. Kawata, "Raman microscopy for dynamic molecular imaging of living cells," *J. Biomed. Opt.* **13**, 044027 (2008).
33. T. Dieing, O. Hollricher, J. Toporski (Eds.) *Confocal Raman Microscopy*, Series in Optical Sciences, Vol. 158 Springer (2011).
34. M. Okada, N. I. Smith, A. F. Palonpon, H. Endo, S. Kawata, M. Sodeoka, K. Fujita, "Label-free Raman observation of cytochrome c dynamics during apoptosis," *Proc. Natl. Acad. Sci. USA* **109**, 28–32 (2012).
35. I. Notingher, C. Green, C. Dyer, E. Perkins, N. Hopkins, C. Lindsay, L. L. Hench, "Discrimination between ricin and sulphur mustard toxicity in vitro using Raman spectroscopy," *J. R. Soc. Interface* **1**, 79–90 (2004).
36. B. R. Wood, D. McNaughton, "Resonance Raman spectroscopy in malaria research," *Expert Rev. Proteomics* **3**, 525–544 (2006).
37. A. J. Hobro, A. Konishi, C. Coban, N. I. Smith, "Raman spectroscopic analysis of malaria disease progression via blood and plasma samples," *Analyst* **138**, 3927–3933 (2013).
38. W. R. Zipfel, R. M. Williams, W. W. Webb, "Nonlinear magic: Multiphoton microscopy in the biosciences," *Nat. Biotechnol.* **21**, 1369–1377 (2003).
39. O. Nadiarnykh, R. B. LaComb, P. J. Campagnola, W. A. Mohler, "Coherent and incoherent SHG in fibrillar cellulose matrices," *Opt. Express* **15**, 3348–3360 (2007).
40. J. Squier, M. Müller, "High resolution nonlinear microscopy: A review of sources and methods for achieving optimal imaging," *Rev. Sci. Instrum.* **72**, 2855–2867 (2001).
41. E. Brown, T. McKee, E. diTomaso, A. Pluen, B. Seed, Y. Boucher, R. K. Jain, "Dynamic imaging of collagen and its modulation in tumors in vivo using second-harmonic generation," *Nat. Methods* **9**, 796–800 (2003).
42. R. M. Williams, W. R. Zipfel, W. W. Webb, "Interpreting second-harmonic generation images of collagen I fibrils," *Biophys. J.* **88**, 1377–1386 (2005).
43. D. A. Dombeck, K. A. Kasischke, H. D. Vishwasrao, M. Ingelsson, B. T. Hyman, W. W. Webb, "Uniform polarity microtubule assemblies imaged in native brain tissue by second-harmonic generation microscopy," *Proc. Natl. Acad. Sci. USA* **100**, 7081–7086 (2003).
44. P. J. Campagnola, L. M. Loew, "Second-harmonic imaging microscopy for visualizing biomolecular arrays in cells, tissues and organisms," *Nat. Biotechnol.* **21**, 1356–1360 (2003).
45. J. Mertz, "Nonlinear microscopy: New techniques and applications," *Curr. Opin. Neurobiol.* **14**, 610–616 (2004).
46. Y. Barad, H. Eisenberg, M. Horowitz, Y. Silberberg, "Nonlinear scanning laser microscopy by third harmonic generation," *Appl. Phys. Lett.* **70**, 922–924 (1997).
47. M. Müller, J. Squier, K. R. Wilson, G. J. Brakenhoff, "3D microscopy of transparent objects using third-harmonic generation," *J. Microsc.* **191**, 266–274 (1998).
48. J. Squier, M. Muller, G. Brakenhoff, K. R. Wilson, "Third harmonic generation microscopy," *Opt. Express* **3**, 315–324 (1998).
49. D. Débarre, W. Supatto, A.-M. Pena, A. Fabre, T. Tordjmann, L. Combettes, M.-C. Schanne-Klein, E. Beaurepaire, "Imaging lipid bodies in cells and tissues using third-harmonic generation microscopy," *Nat. Methods* **3**, 47–53 (2006).
50. N. Olivier, M. A. Luengo-Oroz, L. Duloquin, E. Faure, T. Savy, I. Veilleux, X. Solinas, D. Débarre, P. Bourgine, A. Santos, N. Peyriéras, E. Beaurepaire, "Cell lineage reconstruction of early zebrafish embryos using label-free nonlinear microscopy," *Science* **329**, 967–971 (2010).
51. S. Witte, A. Negrean, J. C. Lodder, C. P. J. de Kock, G. Testa Silva, H. D. Mansvelder, M. Louise Groot, "Label-free live brain imaging and targeted patching with third-harmonic generation microscopy," *Proc. Natl. Acad. Sci. USA* **108**, 5970–5975 (2011).
52. K. König, P. T. C. So, W. W. Mantulin, B. J. Tromberg, E. Gratton, "Two-photon excited lifetime imaging of autofluorescence in cells during UV A and NIR photostress," *J. Microsc.* **183**, 197–204 (1996).
53. S. Huang, A. A. Heikal, W. W. Webb, "Two-photon fluorescence spectroscopy and microscopy of NAD(P)H and flavoprotein," *Biophys. J.* **82**, 2811–2825 (2002).
54. Q. Yu, A. A. Heikal, "Two-photon autofluorescence dynamics imaging reveals sensitivity of intracellular NADH concentration and conformation to cell

J. Innov. Opt. Health Sci. 2014.07. Downloaded from www.worldscientific.com by 103.240.126.9 on 10/21/18. Re-use and distribution is strictly not permitted, except for Open Access articles.

physiology at the single-cell level," *J. Photochem. Photobiol. B, Biol.* **95**, 46–57 (2009).
55. W. Min, C. W. Freudiger, S. Lu, X. S. Xie, "Coherent nonlinear optical imaging: Beyond fluorescence microscopy," *Annu. Rev. Phys. Chem.* **62**, 507–530 (2011).
56. C.-Y. Chung, J. Boik, E. O. Potma, "Biomolecular imaging with coherent nonlinear vibrational microscopy," *Annu. Rev. Phys. Chem.* **64**, 77–99 (2013).
57. L. G. Rodriguez, S. J. Lockett, G. R. Holtom, "Coherent anti-stokes Raman scattering microscopy: A biological review," *Cytometry A* **69A**, 779–791 (2006).
58. C. L. Evans, E. O. Potma, M. Puoris'haag, D. Ct, C. P. Lin, X. S. Xie, "Chemical imaging of tissue in vivo with video-rate coherent anti-Stokes Raman scattering microscopy," *Proc. Natl. Acad. Sci. USA* **102**, 16807–16812 (2005).
59. B. G. Saar, C. W. Freudiger, J. Reichman, C. M. Stanley, G. R. Holtom, X. S. Xie, "Video-rate molecular imaging in vivo with stimulated raman scattering," *Science* **330**, 1368–1370 (2010).
60. M. Flörsheimer, C. Brillert, H. Fuchs, "Chemical imaging of interfaces by sum frequency microscopy," *Langmuir* **15**, 5437–5439 (1999).
61. K. A. Cimatu, S. Baldelli, "Chemical microscopy of surfaces by sum frequency generation imaging " *J. Phys. Chem. C* **113**, 16575–16588 (2009).
62. S. Kogure, K. Inoue, T. Ohmori, M. Ishihara, M. Kikuchi, M. Fujii, M. Sakai, "Infrared imaging of an A549 cultured cell by a vibrational sum-frequency generation detected infrared super-resolution microscope," *Opt. Express* **18**, 13402–13406 (2010).
63. L. V. Wang, "Prospects of photoacoustic tomography," *Med. Phys.* **35**, 5758–5767 (2008).
64. L. V. Wang, "Multiscale photoacoustic microscopy and computed tomography," *Nat. Photonics* **3**, 503–509 (2009).
65. M. Xu, L. V. Wang, "Photoacoustic imaging in biomedicine," *Rev. Sci. Instrum.* **77**, 041101 (2006).
66. C. Zhang, K. Maslov, L. V. Wang, "Subwavelength-resolution label-free photoacoustic microscopy of optical absorption *in vivo*," *Opt. Lett.* **35**, 3195–3197 (2010).
67. C. Zhang, K. Maslov, S. Hu, R. Chen, Q. Zhou, K. Shung, L. V. Wang, "Reflection-mode submicron-resolution in vivo photoacoustic microscopy," *J. Biomed. Opt.* **17**, 20501 (2012).
68. D.-K. Yao, K. Maslov, K. K. Shung, Q. Zhou, L. V. Wang, "*In vivo* label-free photoacoustic microscopy of cell nuclei by excitation of DNA and RNA," *Opt. Lett.* **35**, 4139–4141 (2010).
69. C. Zhang, Y. S. Zhang, D.-K. Yao, Y. Xia, L. V. Wang, "Label-free photoacoustic microscopy of cytochromes," *J. Biomed. Opt.* **18**, 020504–020504 (2013).
70. E. Strohm, E. S. Berndl, M. Kolios, "Probing red blood cell morphology using high-frequency photoacoustics," *Biophys. J.* **105**, 59–67 (2013).
71. V. Zharov, D. Lapotko, "Photothermal imaging of nanoparticles and cells," *IEEE J. Quantum Electron.* **11**, 733–751 (2005).
72. L. Cognet, S. Berciaud, D. Lasne, B. Lounis, "Photothermal methods for single nonluminescent nano-objects," *Anal. Chem.* **80**, 2288–2294 (2008).
73. D. A. Nedosekin, E. I. Galanzha, S. Ayyadevara, R. Shmookler Reis, V. P. Zharov, "Photothermal confocal spectromicroscopy of multiple cellular chromophores and fluorophores," *Biophys. J.* **102**, 672–681 (2012).
74. D. Lasne, G. A. Blab, F. De Giorgi, F. Ichas, B. Lounis, L. Cognet, "Label-free optical imaging of mitochondria in live cells," *Opt. Express* **15**, 14184–14193 (2007).
75. S. Lu, W. Min, S. Chong, G. R. Holtom, X. S. Xie, "Label-free imaging of heme proteins with two-photon excited photothermal lens microscopy," *Appl. Phys. Lett.* **96**, 113701 (2010).
76. E. Shaffer, C. Moratal, P. Magistretti, P. Marquet, C. Depeursinge, "Label-free second-harmonic phase imaging of biological specimen by digital holographic microscopy," *Opt. Lett.* **35**, 4102–4104 (2010).
77. S. Yue, M. Slipchenko, J.-X. Cheng, "Multimodal nonlinear optical microscopy," *Laser Photon. Rev.* **5**, 496–512 (2011).
78. W. R. Zipfel, R. M. Williams, R. Christie, A. Y. Nikitin, B. T. Hyman, W. W. Webb, "Live tissue intrinsic emission microscopy using multi-photon-excited native fluorescence and second harmonic generation," *Proc. Natl. Acad. Sci. USA* **100**, 7075–7080 (2003).
79. J. Adur, V. B. Pelegati, L. F. L. Costa, L. Pietro, A. A. de Thomaz, D. B. Almeida, F. Bottcher-Luiz, L. A. L. A. Andrade, C. L. Cesar, "Recognition of serous ovarian tumors in human samples by multimodal nonlinear optical microscopy," *J. Biomed. Opt.* **16**, 096017 (2011).
80. J. Sun, T. Shilagard, B. Bell, M. Motamedi, G. Vargas, "In vivo multimodal nonlinear optical imaging of mucosal tissue," *Opt. Express* **12**, 2478–2486 (2004).
81. S.-W. Chu, S.-Y. Chen, T.-H. Tsai, T.-M. Liu, C.-Y. Lin, H.-J. Tsai, C.-K. Sun, "In vivo developmental biology study using noninvasive multi-harmonic generation microscopy," *Opt. Express* **11**, 3093–3099 (2003).

J. Innov. Opt. Health Sci. 2014.07. Downloaded from www.worldscientific.com by 103.240.126.9 on 10/21/18. Re-use and distribution is strictly not permitted, except for Open Access articles.


82. W. Supatto, T. V. Truong, D. Débarre, E. Beaurepaire, "Advances in multiphoton microscopy for imaging embryos," *Curr. Opin. Genet. Dev.* **21**, 538–548 (2011).
83. P. Stoller, K. M. Reiser, P. M. Celliers, A. M. Rubenchik, "Polarization-modulated second harmonic generation in collagen," *Biophys. J.* **82**, 3330–3342 (2002).
84. D. Oron, D. Yelin, E. Tal, S. Raz, R. Fachima, Y. Silberberg, "Depth-resolved structural imaging by third-harmonic generation microscopy," *J. Struct. Biol.* **147**, 3–11 (2004).
85. M. Zimmerley, P. Mahou, D. Débarre, M.-C. Schanne-Klein, E. Beaurepaire, "Probing ordered lipid assemblies with polarized third-harmonic-generation microscopy," *Phys. Rev. X* **3**, 011002 (2013).
86. N. Lue, W. Choi, G. Popescu, Z. Yaqoob, K. Badizadegan, R. R. Dasari, M. S. Feld, "Live cell refractometry using hilbert phase microscopy and confocal reflectance microscopy, *J. Phys. Chem. A* **113**, 13327–13330 (2009).
87. E. Shaffer, N. Pavillon, C. Depeursinge, "Single-shot, simultaneous incoherent and holographic microscopy," *J. Microsc.* **245**, 49–62 (2012).
88. T. Colomb, P. Dahlgren, D. Beghuin, E. Cuche, P. Marquet, C. Depeursinge, "Polarization imaging by use of digital holography," *Appl. Opt.* **41**, 27–37 (2002).
89. Y. Kim, J. Jeong, J. Jang, M. W. Kim, Y. Park, "Polarization holographic microscopy for extracting spatio-temporally resolved Jones matrix," *Opt. Express* **20**, 9948–9955 (2012).
90. T. Tahara, Y. Awatsuji, Y. Shimozato, T. Kakue, K. Nishio, S. Ura, T. Kubota, O. Matoba, "Single-shot polarization-imaging digital holography based on simultaneous phase-shifting interferometry," *Opt. Lett.* **36**, 3254–3256 (2011).
91. R. K. Singh, D. N. Naik, H. Itou, Y. Miyamoto, M. Takeda, "Stokes holography," *Opt. Lett.* **37**, 966–968 (2012).
92. M. Villiger, C. Pache, T. Lasser, "Dark-field optical coherence microscopy," *Opt. Lett.* **35**, 3489–3491 (2010).
93. J. F. de Boer, T. E. Milner, "Review of polarization sensitive optical coherence tomography and Stokes vector determination," *J. Biomed. Opt.* **7**, 359–371 (2002).
94. Y. Yasuno, S. Makita, Y. Sutoh, M. Itoh, T. Yatagai, "Birefringence imaging of human skin by polarization-sensitive spectral interferometric optical coherence tomography," *Opt. Lett.* **27**, 1803–1805 (2002).
95. J. Zhang, W. Jung, J. Nelson, Z. Chen, "Full range polarization-sensitive Fourier domain optical coherence tomography," *Opt. Express* **12**, 6033–6039 (2004).
96. W. Oh, S. Yun, B. Vakoc, M. Shishkov, A. Desjardins, B. Park, J. de Boer, G. Tearney, B. Bouma, "High-speed polarization sensitive optical frequency domain imaging with frequency multiplexing," *Opt. Express* **16**, 1096–1103 (2008).
97. Y. Pu, M. Centurion, D. Psaltis, "Harmonic holography: A new holographic principle," *Appl. Opt.* **47**, A103–A110 (2008).
98. E. Shaffer, N. Pavillon, J. Kühn, C. Depeursinge, "Digital holographic microscopy investigation of second harmonic generated at a glass/air interface," *Opt. Lett.* **34**, 2450–2452 (2009).
99. D. G. Winters, D. R. Smith, P. Schlup, R. A. Bartels, "Measurement of orientation and susceptibility ratios using a polarization-resolved second-harmonic generation holographic microscope," *Biomed. Opt. Express* **3**, 2004–2011 (2012).
100. O. Masihzadeh, P. Schlup, R. A. Bartels, "Label-free second harmonic generation holographic microscopy of biological specimens," *Opt. Express* **18**, 9840–9851 (2010).
101. S. Yazdanfar, L. Laiho, P. So, "Interferometric second harmonic generation microscopy," *Opt. Express* **12**, 2739–2745 (2004).
102. S. Yazdanfar, Y. Y. Chen, P. T. So, L. H. Laiho, "Multifunctional imaging of endogenous contrast by simultaneous nonlinear and optical coherence microscopy of thick tissues," *Microsc. Res. Tech.* **70**, 628–633 (2007).
103. Y. Jiang, I. Tomov, Y. Wang, Z. Chen, "Second-harmonic optical coherence tomography," *Opt. Lett.* **29**, 1090–1092 (2004).
104. Y. Jiang, I. V. Tomov, Y. Wang, Z. Chen, "High-resolution second-harmonic optical coherence tomography of collagen in rat-tail tendon," *Appl. Phys. Lett.* **86**, 133901 (2005).
105. M. V. Sarunic, B. E. Applegate, J. A. Izatt, "Spectral domain second-harmonic optical coherence tomography," *Opt. Lett.* **30**, 2391–2393 (2005).
106. J. Su, I. V. Tomov, Y. Jiang, Z. Chen, "High-resolution frequency-domain second-harmonic optical coherence tomography," *Appl. Opt.* **46**, 1770–1775 (2007).
107. K. Kong, C. J. Rowlands, S. Varma, W. Perkins, I. H. Leach, A. A. Koloydenko, H. C. Williams, I. Notingher, "Diagnosis of tumors during tissue-conserving surgery with integrated autofluorescence and Raman scattering microscopy," *Proc. Natl. Acad. Sci. USA* (2013). (in press).
108. J. M. Benevides, S. A. Overman, G. J. Thomas, "Raman, polarized Raman and ultraviolet resonance Raman spectroscopy of nucleic acids and their complexes," *J. Raman Spectrosc.* **36**, 279–299 (2005).

J. Innov. Opt. Health Sci. 2014.07. Downloaded from www.worldscientific.com by 103.240.126.9 on 10/21/18. Re-use and distribution is strictly not permitted, except for Open Access articles.


109. L.-D. Chiu, A. F. Palonpon, K. Hamada, S. Kawata, M. Sodeoka, K. Fujita, "Polarised Raman imaging of living cells for chemical contrast manipulation," *Imaging, Manipulation, and Analysis of Biomolecules, Cells, and Tissues XI*, p. 858720. San Francisco, CA (2013).
110. Y. Saito, M. Kobayashi, D. Hiraga, K. Fujita, S. Kawano, N. I. Smith, Y. Inouye and S. Kawata, "z-Polarization sensitive detection in micro-Raman spectroscopy by radially polarized incident light," *J. Raman Spectrosc.* **39**, 1643–1648 (2008).
111. K. Kneipp, H. Kneipp, I. Itzkan, R. R. Dasari, M. S. Feld, "Surface-enhanced non-linear Raman scattering at the single-molecule level," *Chem. Phys.* **247**, 155–162 (1999).
112. K. Matsuzaki, R. Shimada, H.-O. Hamaguchi, "Superresolution vibrational imaging by simultaneous detection of Raman and hyper-Raman scattering," *Opt. Lett.* **36**, 2545–2547 (2011).
113. J. Kneipp, H. Kneipp, K. Kneipp, "Two-photon vibrational spectroscopy for biosciences based on surface-enhanced hyper-Raman scattering," *Proc. Natl. Acad. Sci. USA* **103**, 17149–17153 (2006).
114. A. Palonpon, T. Ichimura, P. Verma, Y. Inouye, S. Kawata, "Direct evidence of chemical contribution to surface-enhanced hyper-raman scattering," *Appl. Phys. Express* **1**, 092401 (2008).
115. C. A. Patil, N. Bosschaart, M. D. Keller, T. G. van Leeuwen, A. Mahadevan-Jansen, "Combined Raman spectroscopy and optical coherence tomography device for tissue characterization," *Opt. Lett.* **33**, 1135–1137 (2008).
116. C. A. Patil, J. Kalkman, D. J. Faber, J. S. Nyman, T. G. van Leeuwen, A. Mahadevan-Jansen, "Integrated system for combined Raman spectroscopy–spectral domain optical coherence tomography," *J. Biomed. Opt.* **16**, 011007 (2011).
117. J. W. Evans, R. J. Zawadzki, R. Liu, J. W. Chan, S. M. Lane, J. S. Werner, "Optical coherence tomography and Raman spectroscopy of the ex-vivo retina," *J. Biophotonics* **2**, 398–406 (2009).
118. A. Oldenburg, C. Xu, S. Boppart, "Spectroscopic optical coherence tomography and microscopy," *IEEE J. Quantum Electron.* **13**, 1629–1640 (2007).
119. U. Morgner, W. Drexler, F. X. Krtner, X. D. Li, C. Pitris, E. P. Ippen, J. G. Fujimoto, "Spectroscopic optical coherence tomography," *Opt. Lett.* **25**, 111–113 (2000).
120. R. Leitgeb, M. Wojtkowski, A. Kowalczyk, C. K. Hitzenberger, M. Sticker, A. F. Fercher, "Spectral measurement of absorption by spectroscopic frequency-domain optical coherence tomography," *Opt. Lett.* **25**, 820–822 (2000).
121. C. Xu, C. Vinegoni, T. S. Ralston, W. Luo, W. Tan, S. A. Boppart, "Spectroscopic spectral-domain optical coherence microscopy," *Opt. Lett.* **31**, 1079–1081 (2006).
122. C. Xu, F. Kamalabadi, S. A. Boppart, "Comparative performance analysis of time-frequency distributions for spectroscopic optical coherence tomography," *Appl. Opt.* **44**, 1813–1822 (2005).
123. D. Adler, T. Ko, P. Herz, J. Fujimoto, "Optical coherence tomography contrast enhancement using spectroscopic analysis with spectral autocorrelation," *Opt. Express* **12**, 5487–5501 (2004).
124. D. J. Faber, E. G. Mik, M. C. G. Aalders, T. G. van Leeuwen, "Toward assessment of blood oxygen saturation by spectroscopic optical coherence tomography," *Opt. Lett.* **30**, 1015–1017 (2005).
125. J. W. Kang, N. Lue, C.-R. Kong, I. Barman, N. C. Dingari, S. J. Goldfless, J. C. Niles, R. R. Dasari, M. S. Feld, "Combined confocal Raman and quantitative phase microscopy system for biomedical diagnosis," *Biomed. Opt. Express* **2**, 2484–2492 (2011).
126. N. Pavillon, A. J. Hobro, N. I. Smith, "Cell optical density and molecular composition revealed by simultaneous multimodal label-free imaging," *Biophys. J.* **105**, 1123–1132 (2013).
127. C. Yang, A. Wax, I. Georgakoudi, E. B. Hanlon, K. Badizadegan, R. R. Dasari, M. S. Feld, "Interferometric phase-dispersion microscopy," *Opt. Lett.* **25**, 1526–1528 (2000).
128. N. Lue, J. W. Kang, T. R. Hillman, R. R. Dasari, Z. Yaqoob, "Single-shot quantitative dispersion phase microscopy," *Appl. Phys. Lett.* **101**, 084101 (2012).
129. B. Rappaz, F. Charrière, C. Depeursinge, P. J. Magistretti, P. Marquet, "Simultaneous cell morphometry and refractive index measurement with dual-wavelength digital holographic microscopy and dye-enhanced dispersion of perfusion medium," *Opt. Lett.* **33**, 744–746 (2008).
130. Y. Park, T. Yamauchi, W. Choi, R. Dasari, M. S. Feld, "Spectroscopic phase microscopy for quantifying hemoglobin concentrations in intact red blood cells," *Opt. Lett.* **34**, 3668–3670 (2009).
131. F. E. Robles, L. L. Satterwhite, A. Wax, "Nonlinear phase dispersion spectroscopy," *Opt. Lett.* **36**, 4665–4667 (2011).
132. M. Rinehart, Y. Zhu, A. Wax, "Quantitative phase spectroscopy," *Biomed. Opt. Express* **3**, 958–965 (2012).
133. K. Fujita, N. I. Smith, "Label-free molecular imaging of living cells," *Mol. Cells* **26**, 530–535 (2008).
134. D. Li, W. Zheng, Y. Zeng, J. Y. Qu, "In vivo and simultaneous multimodal imaging: Integrated multiplex coherent anti-Stokes Raman scattering

J. Innov. Opt. Health Sci. 2014.07. Downloaded from www.worldscientific.com by 103.240.126.9 on 10/21/18. Re-use and distribution is strictly not permitted, except for Open Access articles.

and two-photon microscopy," *Appl. Phys. Lett.* **97**, 223702 (2010).
135. T. Huff, Y. Shi, Y. Fu, H. Wang, J.-X. Cheng, "Multimodal nonlinear optical microscopy and applications to central nervous system imaging," *IEEE J. Quantum Electron.* **14**, 4–9 (2008).
136. J.-W. Jhan, W.-T. Chang, H.-C. Chen, M.-F. Wu, Y.-T. Lee, C.-H. Chen, I. Liau, "Integrated multiple multi-photon imaging and Raman spectroscopy for characterizing structure-constituent correlation of tissues," *Opt. Express* **16**, 16431–16441 (2008).
137. N. Vogler, A. Medyukhina, I. Latka, S. Kemper, M. Böhm, B. Dietzek, J. Popp, "Towards multimodal nonlinear optical tomography — experimental methodology," *Laser Phys. Lett.* **8**, 617–624 (2011).
138. T. Meyer, O. Guntinas-Lichius, F. von Eggeling, G. Ernst, D. Akimov, M. Schmitt, B. Dietzek, J. Popp, "Multimodal nonlinear microscopic investigations on head and neck squamous cell carcinoma: Toward intraoperative imaging," *Head Neck* **35**, E280–E287 (2013).
139. C.-H. Chien, W.-W. Chen, J.-T. Wu, T.-C. Chang, "Label-free imaging of Drosophila in vivo by coherent anti-Stokes Raman scattering and two-photon excitation autofluorescence microscopy," *J. Biomed. Opt.* **16**, 016012 (2011).
140. H.-W. Wang, T. T. Le, J.-X. Cheng, "Label-free imaging of arterial cells and extracellular matrix using a multimodal CARS microscope," *Opt. Commun.* **281**, 1813–1822 (2008).
141. V. Raghunathan, Y. Han, O. Korth, N.-H. Ge, E. O. Potma, "Rapid vibrational imaging with sum frequency generation microscopy," *Opt. Lett.* **36**, 3891–3893 (2011).
142. H. Chen, H. Wang, M. N. Slipchenko, Y. Jung, Y. Shi, J. Zhu, K. K. Buhman, J.-X. Cheng, "A multimodal platform for nonlinear optical microscopy and microspectroscopy," *Opt. Express* **17**, 1282–1290 (2009).
143. H. Segawa, M. Okuno, H. Kano, P. Leproux, V. Couderc, H.-O. Hamaguchi, "Label-free tetramodal molecular imaging of living cells with CARS, SHG, THG and TSFG (coherent anti-Stokes Raman scattering, second harmonic generation, third harmonic generation and third-order sum frequency generation)," *Opt. Express* **20**, 9551–9557 (2012).
144. J.-X. Cheng, L. D. Book, X. S. Xie, "Polarization coherent anti-Stokes Raman scattering microscopy," *Opt. Lett.* **26**, 1341–1343 (2001).
145. D. L. Marks, S. A. Boppart, "Nonlinear interferometric vibrational imaging," *Phys. Rev. Lett.* **92**, 123905 (2004).
146. E. O. Potma, C. L. Evans, X. S. Xie, "Heterodyne coherent anti-Stokes Raman scattering (CARS) imaging," *Opt. Lett.* **31**, 241–243 (2006).
147. K. Shi, P. S. Edwards, J. Hu, Q. Xu, Y. Wang, D. Psaltis, Z. Liu, "Holographic coherent anti-Stokes Raman scattering bio-imaging," *Biomed. Opt. Express* **3**, 1744–1749 (2012).
148. P. S. Edwards, N. Mehta, K. Shi, Q. Xu, D. Psaltis, Z. Liu, "Coherent anti-Stokes Raman scattering holography: Theory and experiment," *J. Nonlinear Optic. Phys. Mat.* **21**, 1250028 (2012).
149. J. S. Bredfeldt, C. Vinegoni, D. L. Marks, S. A. Boppart, "Molecularly sensitive optical coherence tomography," *Opt. Lett.* **30**, 495–497 (2005).
150. M. Müller, J. M. Schins, "Imaging the thermodynamic state of lipid membranes with multiplex CARS microscopy," *J. Phys. Chem. B* **106**, 3715–3723 (2002).
151. H. Kano, H.-O. Hamaguchi, "In-vivo multi-nonlinear optical imaging of a living cell using a supercontinuum light source generated from a photonic crystal fiber," *Opt. Express* **14**, 2798–2804 (2006).
152. J. Y. Lee, S.-H. Kim, D. W. Moon, E. S. Lee, "Three-color multiplex CARS for fast imaging and microspectroscopy in the entire CHn stretching vibrational region," *Opt. Express* **17**, 22281–22295 (2009).
153. M. Okuno, H. Kano, P. Leproux, V. Couderc, H.-O. Hamaguchi, "Ultrabroadband multiplex CARS microspectroscopy and imaging using a subnanosecond supercontinuum light source in the deep near infrared," *Opt. Lett.* **33**, 923–925 (2008).
154. K. Furusawa, N. Hayazawa, S. Kawata, "Two-beam multiplexed CARS based on a broadband oscillator," *J. Raman Spectrosc.* **41**, 840–847 (2010).
155. D. Fu, G. Holtom, C. Freudiger, X. Zhang, X. S. Xie, "Hyperspectral imaging with stimulated Raman scattering by chirped femtosecond lasers," *J. Phys. Chem. B* **117**, 4634–4640 (2012).
156. L. Kong, M. Ji, G. R. Holtom, D. Fu, C. W. Freudiger, X. S. Xie, "Multicolor stimulated Raman scattering microscopy with a rapidly tunable optical parametric oscillator," *Opt. Lett.* **38**, 145–147 (2013).
157. D. Fu, F.-K. Lu, X. Zhang, C. Freudiger, D. R. Pernik, G. Holtom, X. S. Xie, "Quantitative chemical imaging with multiplex stimulated Raman scattering microscopy," *J. Am. Chem. Soc.* **134**, 3623–3626 (2012).
158. C. Krafft, B. Dietzek, J. Popp, "Raman and CARS microspectroscopy of cells and tissues," *Analyst* **134**, 1046–1057 (2009).

J. Innov. Opt. Health Sci. 2014.07. Downloaded from www.worldscientific.com by 103.240.126.9 on 10/21/18. Re-use and distribution is strictly not permitted, except for Open Access articles.


159. W. Benalcazar, P. Chowdary, Z. Jiang, D. Marks, E. Chaney, M. Gruebele, S. Boppart, "High-speed nonlinear interferometric vibrational imaging of biological tissue with comparison to Raman microscopy," *IEEE J. Quantum Electron.* **16**, 824–832 (2010).
160. A. Downes, R. Mouras, P. Bagnaninchi, A. Elfick, "Raman spectroscopy and CARS microscopy of stem cells and their derivatives," *J. Raman Spectrosc.* **42**, 1864–1870 (2011).
161. X. N. He, J. Allen, P. N. Black, T. Baldacchini, X. Huang, H. Huang, L. Jiang, Y. F. Lu, "Coherent anti-Stokes Raman scattering and spontaneous Raman spectroscopy and microscopy of microalgae with nitrogen depletion," *Biomed. Opt. Express* **3**, 2896–2906 (2012).
162. T. Meyer, N. Bergner, C. Bielecki, C. Krafft, D. Akimov, B. F. M. Romeike, R. Reichart, R. Kalff, B. Dietzek, J. Popp, "Nonlinear microscopy, infrared, and Raman microspectroscopy for brain tumor analysis," *J. Biomed. Opt.* **16**, 021113 (2011).
163. C. Krafft, B. Dietzek, M. Schmitt, J. Popp, "Raman and coherent anti-Stokes Raman scattering microspectroscopy for biomedical applications," *J. Biomed. Opt.* **17**, 040801 (2012).
164. S. Jiao, Z. Xie, H. F. Zhang, C. A. Puliafito, "Simultaneous multimodal imaging with integrated photoacoustic microscopy and optical coherence tomography," *Opt. Lett.* **34**, 2961–2963 (2009).
165. X. Zhang, H. F. Zhang, S. Jiao, "Optical coherence photoacoustic microscopy: Accomplishing optical coherence tomography and photoacoustic microscopy with a single light source," *J. Biomed. Opt.* **17**, 030502 (2012).
166. Z. Tan, Z. Tang, Y. Wu, Y. Liao, W. Dong, L. Guo, "Multimodal subcellular imaging with microcavity photoacoustic transducer," *Opt. Express* **19**, 2426–2431 (2011).
167. V. Ntziachristos, D. Razansky, "Molecular imaging by means of multispectral optoacoustic tomography (MSOT)," *Chem. Rev.* **110**, 2783–2794 (2010).
168. J. Yao, L. V. Wang, "Photoacoustic tomography: Fundamentals, advances and prospects," *Contrast Media Mol. Imaging* **6**, 332–345 (2011).
169. Y. Yamaoka, M. Nambu, T. Takamatsu, "Fine depth resolution of two-photon absorption-induced photoacoustic microscopy using low-frequency bandpass filtering," *Opt. Express* **19**, 13365–13377 (2011).
170. V. V. Yakovlev, H. F. Zhang, G. D. Noojin, M. L. Denton, R. J. Thomas, M. O. Scully, "Stimulated Raman photoacoustic imaging," *Proc. Natl. Acad. Sci. USA* **107**, 20335–20339 (2010).
171. H.-W. Wang, N. Chai, P. Wang, S. Hu, W. Dou, D. Umulis, L. V. Wang, M. Sturek, R. Lucht, J.-X. Cheng, "Label-free bond-selective imaging by listening to vibrationally excited molecules," *Phys. Rev. Lett.* **106**, 238106 (2011).
172. Y. Park, G. Popescu, K. Badizadegan, R. R. Dasari, M. S. Feld, "Diffraction phase and fluorescence microscopy," *Opt. Express* **14**, 8263–8268 (2006).
173. N. Pavillon, A. Benke, D. Boss, C. Moratal, J. Kühn, P. Jourdain, C. Depeursinge, P. J. Magistretti, P. Marquet, "Cell morphology and intracellular ionic homeostasis explored with a multimodal approach combining epifluorescence and digital holographic microscopy," *J. Biophotonics* **3**, 432–436 (2010).
174. C. Yang, "Molecular contrast optical coherence tomography: A review," *Photochem. Photobiol.* **81**, 215–237 (2005).
175. E. Beaurepaire, L. Moreaux, F. Amblard, J. Mertz, "Combined scanning optical coherence and two-photon-excited fluorescence microscopy," *Opt. Lett.* **24**, 969–971 (1999).
176. C. Vinegoni, T. Ralston, W. Tan, W. Luo, D. L. Marks, S. A. Boppart, "Integrated structural and functional optical imaging combining spectral-domain optical coherence and multiphoton microscopy," *Appl. Phys. Lett.* **88**, 053901 (2006).
177. S. Tang, C.-H. Sun, T. B. Krasieva, Z. Chen, B. J. Tromberg, "Imaging subcellular scattering contrast by using combined optical coherence and multiphoton microscopy," *Opt. Lett.* **32**, 503–505 (2007).
178. V. V. Pully, A. Lenferink, C. Otto, "Hybrid Rayleigh, Raman and two-photon excited fluorescence spectral confocal microscopy of living cells," *J. Raman Spectrosc.* **41**, 599–608 (2010).
179. V. Pully, A. Lenferink, C. Otto, "Raman-fluorescence hybrid microspectroscopy of cell nuclei," *Vib. Spectrosc.* **53**, 12–18 (2010).
180. R. Carriles, D. N. Schafer, K. E. Sheetz, J. J. Field, R. Cisek, V. Barzda, A. W. Sylvester, J. A. Squier, "Invited review article: Imaging techniques for harmonic and multiphoton absorption fluorescence microscopy," *Rev. Sci. Instrum.* **80**, 081101r (2009).
181. T. Abraham, S. Wadsworth, J. M. Carthy, D. V. Pechkovsky, B. McManus, "Minimally invasive imaging method based on second harmonic generation and multiphoton excitation fluorescence in translational respiratory research," *Respirology* **16**, 22–33 (2011).
182. V. B. Pelegati, J. Adur, A. A. De Thomaz, D. B. Almeida, M. O. Baratti, L. A. L. A. Andrade, F. Bottcher-luiz, C. L. Cesar, "Harmonic optical microscopy and fluorescence lifetime imaging platform for multimodal imaging," *Microsc. Res. Tech.* **75**, 1383–1394 (2012).

J. Innov. Opt. Health Sci. 2014.07. Downloaded from www.worldscientific.com
by 103.240.126.9 on 10/21/18. Re-use and distribution is strictly not permitted, except for Open Access articles.

183. L. Tong, J.-X. Cheng, "Label-free imaging through nonlinear optical signals," *Mater. Today* **14**, 264–273 (2011).
184. A. S. Stender, K. Marchuk, C. Liu, S. Sander, M. W. Meyer, E. A. Smith, B. Neupane, G. Wang, J. Li, J.-X. Cheng, B. Huang, N. Fang, "Single cell optical imaging and spectroscopy," *Chem. Rev.* **113**, 2469–2527 (2013).
185. J. B. Pawley (Ed.) *Handbook of Biological Confocal Microscopy*, 3rd Edition, Springer, New York (2006).
186. B. W. Schilling, T.-C. Poon, G. Indebetouw, B. Storrie, K. Shinoda, Y. Suzuki, M. H. Wu, "Three-dimensional holographic fluorescence microscopy," *Opt. Lett.* **22**, 1506–1508 (1997).
187. G. Indebetouw, W. Zhong, "Scanning holographic microscopy of three-dimensional fluorescent specimens," *J. Opt. Soc. Am. A* **23**, 1699–1707 (2006).
188. A. Bilenca, J. Cao, M. Colice, A. Ozcan, B. Bouma, L. Raftery, G. Tearney, "Fluorescence interferometry," *Ann. N. Y. Acad. Sci.* **1130**, 68–77 (2008).
189. J. Rosen, G. Brooker, "Fluorescence incoherent color holography," *Opt. Express* **15**, 2244–2250 (2007).
190. J. Rosen, G. Brooker, "Non-scanning motionless fluorescence three-dimensional holographic microscopy," *Nat. Photonics* **2**, 190–195 (2008).
191. H. Yamakoshi, K. Dodo, A. Palonpon, J. Ando, K. Fujita, S. Kawata, M. Sodeoka, "Alkyne-tag Raman imaging for visualization of mobile small molecules in live cells," *J. Am. Chem. Soc.* **134**, 20681–20689 (2012).
192. C.-L. Hsieh, R. Grange, Y. Pu, D. Psaltis, "Three-dimensional harmonic holographic microcopy using nanoparticles as probes for cell imaging," *Opt. Express* **17**, 2880–2891 (2009).
193. R. Grange, T. Lanvin, C.-L. Hsieh, Y. Pu, D. Psaltis, "Imaging with second-harmonic radiation probes in living tissue," *Biomed. Opt. Express* **2**, 2532–2539 (2011).
194. Y. Pu, D. Psaltis, "Seeing through turbidity with harmonic holography [Invited]," *Appl. Opt.* **52**, 567–578 (2013).
195. C.-L. Hsieh, Y. Pu, R. Grange, G. Laporte, D. Psaltis, "Imaging through turbid layers by scanning the phase conjugated second harmonic radiation from a nanoparticle," *Opt. Express* **18**, 20723–20731 (2010).
196. X. Yang, C.-L. Hsieh, Y. Pu, D. Psaltis, "Three-dimensional scanning microscopy through thin turbid media," *Opt. Express* **20**, 2500–2506 (2012).
197. B. A. Nemet, V. Nikolenko, R. Yuste, "Second harmonic imaging of membrane potential of neurons with retinal," *J. Biomed. Opt.* **9**, 873–881 (2004).
198. D. S. Peterka, H. Takahashi, R. Yuste, "Imaging voltage in neurons," *Neuron* **69**, 9–21 (2011).
199. M. Nuriya, J. Jiang, B. Nemet, K. B. Eisenthal, R. Yuste, "Imaging membrane potential in dendritic spines," *Proc. Natl. Acad. Sci. USA* **103**, 786–790 (2006).
200. P. Theer, W. Denk, M. Sheves, A. Lewis, P. B. Detwiler, "Second-harmonic generation imaging of membrane potential with retinal analogues," *Biophys. J.* **100**, 232–242 (2011).